HHS Public Access

Author manuscript

*Abdom Radiol (NY)*. Author manuscript; available in PMC 2023 July 01.

Published in final edited form as:

*Abdom Radiol (NY)*. 2022 July ; 47(7): 2420–2441. doi:10.1007/s00261-022-03540-2.

# Spilling the Beans: An Inside Scoop on the Imaging of Renal Parenchymal Disease

**Joel Thomas, MD**,
Mallinckrodt Institute of Radiology, Washington University School of Medicine, 510 S Kingshighway Blvd, St. Louis, MO 63110.

**Daniel R. Ludwig, MD**,
Abdominal Imaging, Mallinckrodt Institute of Radiology, Washington University School of Medicine, 510 S Kingshighway Blvd, St. Louis, MO 63110.

**David H. Ballard, MD**,
Abdominal Imaging, Mallinckrodt Institute of Radiology, Washington University School of Medicine, 510 S Kingshighway Blvd, St. Louis, MO 63110.

**Vincent M. Mellnick, MD**,
Abdominal Imaging, Mallinckrodt Institute of Radiology, Washington University School of Medicine, 510 S Kingshighway Blvd, St. Louis, MO 63110.

**Cary L. Siegel, MD**,
Abdominal Imaging, Mallinckrodt Institute of Radiology, Washington University School of Medicine, 510 S Kingshighway Blvd, St. Louis, MO 63110.

**Tyler J. Fraum, MD**
Abdominal Imaging & Nuclear Medicine, Mallinckrodt Institute of Radiology, Washington University School of Medicine, 510 S Kingshighway Blvd, St. Louis, MO 63110.

## Abstract

Renal parenchymal disease is commonly encountered on imaging, and an understanding of the spectrum of pathology is vital to making correct diagnoses and recommendations for management. These conditions can be categorized based on the presence of calcifications, cysts, solid masses, patterns of enhancement, and other characteristic non-mass findings, as well as on their spatial distribution (i.e., medullary vs. cortical). Making an accurate diagnosis is often challenging, as there is overlap in the features of various diseases, and many benign entities may mimic pathology.

**Corresponding author:** Joel Thomas, MD – joel.t@wustl.edu. 314-276-7570.
Author Competing Interests:

1. JT: None
2. DRL: None
3. DHB: During the study period, received salary support from National Institutes of Health TOP-TIER grant T32-EB021955
4. VMM: None
5. CLS: None
6. TJF: Consultant, Arterys Inc; Research Support, Siemens Healthineers; Honoraria, PrecisCa Oncology

This review broadly discusses imaging features of renal parenchymal disease and provides a systematic approach to characterize findings and appropriately guide further management.

**Keywords**

kidneys; renal; nephrocalcinosis; renal cell carcinoma; cysts

## Introduction

Renal parenchymal findings are commonly encountered on ultrasound, computed tomography, and magnetic resonance imaging of the abdomen. The spectrum of findings is broad, and there is significant overlap in the imaging characteristics of benign and pathologic entities. Additionally, the majority of incidentally discovered renal findings are benign cysts [1], and therefore the challenge remains to identify which findings warrant further follow-up.

Broadly speaking, renal parenchymal findings can be categorized based on the presence of calcifications, cysts, solid masses, patterns of enhancement, and other non-mass findings, as well as on their spatial distribution (i.e., medullary vs. cortical) (Table 1). Understanding the pathophysiology of common conditions as it relates to renal anatomy and physiology will also assist in diagnosis. The purpose of this review is to provide a systematic approach to characterize renal parenchymal imaging findings to appropriately narrow the differential diagnosis for further management.

## Relevant Renal Anatomy & Physiology

Basic knowledge of the gross and microscopic anatomy of the kidney is essential to understanding patterns of renal parenchymal disease (Figure 1). The kidney is divided into the cortex peripherally and medulla centrally, with the latter consisting predominantly of medullary pyramids with interposed thin strips of cortical tissue called columns of Bertin. The tip of the medullary pyramid, called the papilla, protrudes into a minor calyx. Minor calyces coalesce into major calyces, which empty into the renal pelvis and thence into the ureter.

The functional unit of the kidney is the nephron, which spans the cortex and medulla [2]. The glomerulus, a tuft of fenestrated capillaries located in the renal cortex, produces an ultrafiltrate of blood while preventing the loss of proteins and blood cells. This ultrafiltrate (~180 L/day) is collected by Bowman’s capsule and conveyed to the proximal tubule, where approximately two-thirds of the filtered sodium and water and other filtered substances (e.g., glucose, amino acids) are resorbed. From the proximal tubule, the ultrafiltrate passes into the medulla via the loop of Henle. Here, additional water is resorbed by means of medullary hyperosmolarity and collected by the vasa recta, a delicate capillary bed surrounding the loop of Henle. The ultrafiltrate is then transported back into the cortex to the distal tubule, where additional water and sodium is resorbed. Finally, the ultrafiltrate passes into the medulla again via the collecting duct, which is lined by two types of cells. The principal cells, which are regulated by antidiuretic hormone, are responsible for sodium and water

absorption. The α-intercalated cells are responsible for potassium resorption and acid (i.e., $H^+$) secretion. The collecting duct empties into minor calyx the papilla, at which point the ultrafiltrate is considered urine.

Note that the glomerulus, Bowman's capsule, and proximal/distal tubules are cortical structures, whereas the loop of Henle, collecting duct, and papilla are medullary structures. This dichotomy is important to remember in formulating a differential diagnosis when encountering a patient with suspected renal parenchymal disease.

## CALCIFIC DISEASES

Nephrocalcinosis refers to generalized deposition of calcium (i.e, calcium oxalate or calcium phosphate) within the renal parenchyma which may be caused by a variety of etiologies. It is an insidious process that is preceded by microscopic accumulation of calcium before it becomes evident on imaging [3]. When parenchymal calcifications are identified, radiologists should first determine whether they are predominantly medullary, predominantly cortical, or combined (i.e., both medullary and cortical). Additionally, one should be mindful of common mimics of nephrocalcinosis, as will be discussed. Medullary nephrocalcinosis (97% of cases) is much more common than cortical nephrocalcinosis (< 3%); the combined form of medullary and cortical nephrocalcinosis is extremely rare (< 1%), though these data are based on a study from 1976 [4]. Given the rarity of combined medullary/cortical nephrocalcinosis and the significantly higher prevalence of medullary nephrocalcinosis, the possibility of medullary nephrocalcinosis with associated cortical atrophy producing the spurious appearance of combined medullary/cortical nephrocalcinosis should be considered when encountering an apparent case of combined medullary/cortical nephrocalcinosis. The calcific renal diseases are summarized in Figure 2.

### Medullary nephrocalcinosis

Medullary nephrocalcinosis (Figure 3a-d) is best identified by hyperdense medullary pyramids on noncontrast CT, as contrast material can obscure or even mimic nephrocalcinosis. On ultrasound, the typical appearance is hyperechoic medullary pyramids with posterior acoustic shadowing.

On magnetic resonance imaging (MRI), the classical appearance is T1-hypointense, T2-hypointense medullary pyramids due to calcium-related dephasing and signal loss. Occasionally, it may present as T1-hyperintense medullary pyramids due to T1-shortening effects of calcium on surrounding water molecules. The differential diagnosis for medullary nephrocalcinosis includes common entities such as hyperparathyroidism and medullary sponge kidney, as well as uncommon entities such as distal renal tubular acidosis, other causes of hypercalcemia (e.g., hypervitaminosis D, milk-alkali syndrome, sarcoidosis), hyperthyroidism or hypothyroidism, long-term furosemide abuse, Bartter syndrome, Liddle syndrome, and renal papillary necrosis.

**Medullary sponge kidney—**Medullary sponge kidney (MSK) is a congenital disorder characterized by dilation of the collecting ducts of the renal pyramids, resulting in a sponge-like appearance on gross pathology. The pathophysiology involves relative stasis of urine

in the dilated medullary collecting ducts, which predisposes to stone precipitation, resulting in medullary calcifications (Figure 4a-c). Most cases are asymptomatic, but patients are at increased risk for nephrolithiasis and urinary tract infection. It likely has a genetic component given its association with Ehlers-Danlos syndrome, Beckwith-Wiedemann syndrome, Caroli's disease, and Wilms tumor [5,6].

MSK may affect the kidneys asymmetrically or segmentally, and it may even involve a single medullary pyramid. In contrast, calcifications seen with other causes of medullary nephrocalcinosis are usually symmetric and diffuse. The presence of medullary-predominant cysts is also a common finding that can help distinguish it from other etiologies of medullary nephrocalcinosis. On excretory phase images, contrast within the dilated collecting ducts confers a paintbrush appearance to the medullary pyramids [7].

**Tubular ectasia—**An important mimic of MSK is tubular ectasia, also known as "benign renal tubular ectasia" – to distinguish it from MSK, which is more likely to be associated with complications such as stone-related obstruction or infection. That said, tubular ectasia may represent a *forme fruste* of MSK. As in MSK, tubular ectasia is characterized by dilation of the collecting ducts resulting in linear collections of contrast material in the medullary pyramids that produce a 'paintbrush' appearance on excretory phase computed tomography (Figure 4d-e). In contrast to MSK, tubular ectasia lacks medullary nephrocalcinosis and medullary-predominant cysts [8].

**Hyperparathyroidism—**In hyperparathyroidism, excess parathyroid hormone induces hypercalcemia and, consequently, hypercalciuria. Elevated calcium levels in the urine predispose to calcium oxalate and calcium phosphate precipitation, resulting in medullary nephrocalcinosis that is often symmetric and diffuse (Figure 5a). Other imaging features associated with hyperparathyroidism (e.g., rugger jersey spine) may also be present [9]. Hyperparathyroidism most commonly occurs in isolation [10], but a minority of cases arise in the setting of inherited syndromes such as multiple endocrine neoplasia 1 and 2A. In such cases, other findings of multiple neuroendocrine neoplasia type 2 (e.g., post-surgical changes in the thyroid or adrenal bed) may suggest inherited syndromic hyperparathyroidism as the etiology of medullary nephrocalcinosis (Figure 5b-c).

**Type I (distal) renal tubular acidosis—**Type I (distal) renal tubular acidosis refers to an array of hereditary and acquired disorders resulting in impaired H+ secretion by the collecting ducts [11]. The resulting alkaline state of the urine in the collecting ducts promotes precipitation of calcium phosphate, resulting in medullary nephrocalcinosis (Figure 5d). As in hyperparathyroidism, medullary calcifications are typically symmetric and diffuse. It is associated with autoimmune disease, including Sjögren syndrome, rheumatoid arthritis, and systemic lupus erythematosus.

**Mimics of medullary nephrocalcinosis: alkaline-encrusted pyelitis and dehydration—**Alkaline-encrusted pyelitis typically affects debilitated patients following urological procedures. It arises from chronic infection with urease-positive organisms, often *Corynebacterium urealyticum*. When this diagnosis is suspected at imaging, radiologists should suggest specifically culturing for *Corynebacterium urealyticum*. Urease splits urea

into ammonia, resulting in more alkaline urine, which promotes urothelial deposition of calcium phosphate and struvite crystals. Alkaline-encrusted pyelitis commonly occurs in with the setting of chronic indwelling urethral or suprapubic catheters and nephroureteral stents. CT is the primary modality to see the characteristic imaging features of alkaline-encrusted pyelitis [12,13]. Calcifications will deposit along the urothelium (Figure 6a), in contrast to the medullary pattern of hyperattenuation at CT for nephrocalcinosis. When alkaline deposition occurs at the proximal urothelium (e.g., the minor calyx), the appearance should not be mistaken for calcification of the medullary pyramid as in medullary nephrocalcinosis. The peripheral calcifications may also mimic numerous small non-obstructing stones within the collecting system; multiplanar reformations can be used to demonstrate the close association of alkaline-encrusted pyelitis to the urothelial wall [12], whereas urolithiasis would be more likely to occupy the lumen of the collecting system. Similar calcifications may also affect the urinary bladder (i.e., alkaline-encrusted cystitis), which may help distinguish it from nephrocalcinosis.

Another mimic of medullary nephrocalcinosis radiologists might encounter is hyperattenuation of the renal medullary pyramids related to a dehydrated state [14]. At noncontrast CT, this condition manifests as relative hyperdensity of the renal medullary pyramids compared with the cortex. In the setting of acute water restriction, healthy subjects with normal renal function have been shown to develop medullary pyramid hyperdensity on noncontrast CT that resolves with rehydration [15]. The underlying mechanism is unclear but may relate to greater concentration of the urine by the loops of Henle and collecting ducts, as the kidneys act to minimize excretion of water. The resulting hyperdensity of the medullary pyramids (Figure 6b) related to dehydration may resemble medullary nephrocalcinosis but should appear more vague than true calcification and should not persist over time [16]. Follow-up imaging with ultrasound may be helpful to rule out medullary nephrocalcinosis in equivocal cases.

## Cortical nephrocalcinosis

Relatively common pathologies (e.g., acute cortical necrosis and chronic glomerulonephritis, chronic renal transplant rejection) or rare conditions (e.g., autosomal recessive polycystic kidney disease, Alport syndrome) can manifest with cortical nephrocalcinosis.

**Chronic glomerulonephritis—**Recall that glomeruli are cortical structures. As such, chronic immune-mediated damage may result in glomerular necrosis, with subsequent development of dystrophic cortical calcifications (Figure 7a-b). There may also be associated renal atrophy. Glomerulonephritis has numerous potential etiologies; some of these entities have additional radiological manifestations that can support an imaging diagnosis of chronic glomerulonephritis when present in association with cortical nephrocalcinosis. These entities include granulomatosis with polyangiitis (associated with peripheral-predominant pulmonary consolidation or nodules/masses – often cavitary), systemic lupus erythematosus (associated with serositis, e.g., pleural or pericardial effusion) (Figure 7a-b); and anti-glomerular basement membrane disease (associated with pulmonary hemorrhage), among others.

**Acute cortical necrosis (sequelae)—**Renal cortical necrosis typically results from acute ischemia of the renal cortex related to compromised arterial inflow, often secondary to systemic arterial hypotension. The most frequent etiologies include pregnancy-related hemorrhage, sepsis, and trauma. The acute phase is characterized by focal or diffuse cortical hypoenhancement (often bilateral) (Figure 7c), potentially associated with a thin line of preserved perfusion at the capsule (i.e., cortical rim sign). Subsequently, dystrophic cortical calcifications (Figure 7d) develop in the areas of necrosis, resulting in cortical nephrocalcinosis [17].

**Chronic transplant rejection—**Renal transplant rejection preferentially involves the renal cortex [18,19], and chronic transplant rejection promotes dystrophic calcification that can manifest as cortical nephrocalcinosis [20,21]. Necrosis of cortical tissue promotes dystrophic calcification, eventually resulting in cortical nephrocalcinosis (Figure 7e). These cortical calcifications can take months to years to become apparent on imaging, lagging behind clinically apparent declines in renal function.

**Mimic of cortical nephrocalcinosis: acute tubular necrosis—**In acute tubular necrosis (ATN), ischemic or toxic insults cause necrosis of renal tubular cells, resulting in the deposition of cellular debris in the tubules. This debris impedes the excretion of contrast material (or radiotracer) from the renal parenchyma into the calyces. ATN classically manifests as a persistent nephrogram on a non-contrast CT scan performed after a recent contrast-enhanced CT. Contrast retention can be diffuse and uniform or asymmetric and patchy (Figure 8a). Occasionally, the contrast retention associated with ATN can have an atypical cortical-predominant pattern (Figure 8b-c) that can be confused with cortical nephrocalcinosis on a noncontrast examination. When seen, vicarious biliary excretion of contrast (usually most evident in gallbladder) supports a diagnosis of ATN rather than nephrocalcinosis. Nephrocalcinosis should persist over time, whereas contrast retention will eventually resolve as renal function recovers [22].

## Cortical and medullary nephrocalcinosis

Keeping in mind that combined cortical/medullary nephrocalcinosis is extremely uncommon, the differential diagnosis includes oxalosis and prior mycobacterial infection.

**Oxalosis—**Hyperoxaluria refers to elevated oxalate levels in the urine. Primary hyperoxaluria is caused by a genetic defect resulting in overproduction of oxalate. Secondary hyperoxaluria can be caused by an acquired defect resulting in increased absorption of oxalate (e.g., Crohn’s disease, short gut syndrome) or improper processing of oxalate (e.g., end-stage renal disease and chronic liver disease). Hyperoxaluria promotes the formation of calcium oxalate in the kidneys, manifesting as nephrocalcinosis and/or nephrolithiasis. Oxalosis often manifests as diffuse uniform deposition of calcium throughout the entire kidney (Figure 9a), though patchy and cortical-predominant forms can be seen. Renal oxalate deposition can result in renal failure, leading to oxalate accumulation in other organs as a primary means of oxalate excretion is lost [23].

**Tuberculosis and atypical mycobacteria—**Typical and atypical mycobacterial infections are etiologies that may lead to the imaging appearance of combined cortical/medullary nephrocalcinosis [24]. The genitourinary tract accounts for 4-8% of extrapulmonary tuberculosis infections. The bacilli reach kidneys via hematogenous spread from lungs, forming granulomas in the cortex adjacent to glomeruli. Reactivation can result in spread via glomeruli into nephrons, with distribution throughout cortex/medulla and eventually into collecting system. Renal calcifications develop in approximately 50% of cases. In early disease, one may see patchy and punctate calcifications, often associated with hydronephrosis related to strictures of the collecting system. In late disease, one may see diffuse, dense, dystrophic calcifications (i.e., “putty kidney”) (Figure 9b) [25].

At CT, combined cortical/medullary nephrocalcinosis will manifest as calcifications throughout the cortex and medulla [23,25]. Radiologists should be aware of the rarity of the combined cortical/medullary form of nephrocalcinosis. As medullary nephrocalcinosis is much more common, the differential diagnosis for apparent combined cortical/medullary nephrocalcinosis should include medullary nephrocalcinosis with concurrent cortical atrophy.

Double-obliquing the kidneys to view an orthogonal coronal view may be helpful in distinguishing cortical/medullary nephrocalcinosis due to mycobacterial infection versus oxalosis. CT-evident calcifications in combined cortical/medullary nephrocalcinosis will typically be punctate with many individual calcifications when due to mycobacterial infection versus more uniformly and diffusely calcified when due to oxalosis [23]. The lobulated, densely calcified appearance of a putty kidney is an extreme example of end-stage mycobacterial renal involvement, whereas a diffusely calcified atrophic kidney with a smooth external contour is more typical of oxalosis [25,26].

## CYSTIC DISEASES

The renal cystic diseases can be categorized in a variety of ways according to cause (hereditary versus acquired), location (cortical, medullary, or diffuse), and size (microcysts vs. macrocysts). For the purposes of this section, we will categorize cystic renal disease based on size and location (Figure 10). Here, we define microcysts as less than 1 cm and macrocysts as greater than 1 cm in diameter [27,28].

### Microcysts

The differential diagnosis for a kidney with numerous cysts – the majority of which are less than 1 cm in diameter –includes glomerulocystic kidney disease, lithium nephrotoxicity, medullary cystic disease, and autosomal recessive polycystic kidney disease.

**Lithium nephrotoxicity—**Lithium has long been used as a treatment for mood disorders, particularly bipolar disorder. It has a narrow therapeutic window with the potential for a wide array of side effects in multiple organ systems. In the kidneys, lithium can potentially cause diabetes insipidus and acute renal failure. Chronic lithium use results in renal tubular atrophy, glomerulosclerosis, fibrosis, and tubular dilatation, leading to microcyst formation (Figure 11a-b). The cysts are distributed in the cortex and medulla, and often 1-2 mm in

size. The cysts may also be accompanied by punctate calcifications [29]. However, the key to making this diagnosis is correlation with a history of bipolar disorder and/or lithium use.

**Glomerulocystic kidney disease—**Glomerulocystic kidney disease (GCKD) may arise either sporadically or heritably. It occurs due to dilatation of Bowman's capsule, resulting in tiny, cortically-based cysts. The characteristic subcapsular location of the cysts is an important clue to this diagnosis (Figure 11c) [30]. GCKD may be accompanied by renal atrophy, leading to renal failure. GCKD often occurs in children but may not present until adulthood. On occasion, it may be seen in conjunction with tuberous sclerosis.

**Medullary cystic disease—**Medullary cystic disease is hereditary and most commonly presents in children and occurs due to chronic tubulointerstitial nephritis and progressive tubular atrophy. The disease may also be clinically associated with nephronophthisis, leading to polydipsia, polyuria, fatigue, and weakness. When this occurs along with medullary cystic disease, it is termed medullary cystic disease complex, a common cause for end-stage renal disease in young adulthood [31]. Radiologically, this entity manifests as multiple cysts centered at the renal corticomedullary junction (Figure 11d). Although the cysts are often small (i.e., microcysts), they may be up to 1.5 cm in size. The affected kidneys may be small as well due to parenchymal fibrosis. Echogenicity of the kidneys affected by medullary cystic disease may also be increased when imaged with ultrasound.

**Autosomal Recessive Polycystic Kidney Disease (ARPKD)—**ARPKD is less common than ADPKD and typically diagnosed earlier, potentially in utero due to oligohydramnios. Severe renal dysfunction usually occurs within the first month of life. Affected patients often present with bulging flanks due to marked renal enlargement. The kidneys may have microcysts distributed throughout the renal cortex and medulla (Figure 11e-f), but because of their small size, microcysts associated with ARPKD are often not apparent on imaging [32]. Extrarenal abnormalities associated with ARPKD include congenital hepatic fibrosis and Caroli's disease.

## Macrocysts

The differential diagnosis for kidneys with numerous cysts – the majority of which are greater than 1 cm in diameter –includes autosomal dominant polycystic kidney disease and acquired cystic kidney disease. Note that it can be challenging to differentiate the macrocystic diseases from otherwise normal kidneys with multiple sporadic cysts. As discussed below, the presence of cysts in other organs, family history of renal disease, or known chronic kidney disease can be helpful supplements to the imaging findings.

**Autosomal Dominant Polycystic Kidney Disease (ADPKD)—**ADPKD is a relatively common genetic disorder, affecting roughly 1 in 500 people and accounting for 5-10% of individuals with end-stage renal disease. Although most cases of ADPKD are inherited, up to 15% of affected patients may have no identifiable family history. There are at least 2 major phenotypes of ADPKD. Most patients (85%) have a mutation in PKD1, which is associated with more severe renal disease. Mutations in PKD2 are associated with

a less severe phenotype [33]. Most patients are diagnosed when screened after a family member is diagnosed with the condition.

In the absence of family history, it may be challenging to distinguish ADPKD from multiple sporadic renal cysts. Fortunately, there are age-dependent ultrasound criteria for the diagnosis of the common PKD1 phenotype [33]. For at-risk patients between aged 15-29 years, the presence of at least 2 (unilateral or bilateral) renal cysts is sufficient for diagnosis. For patients aged 30-59 years, the presence of at least 2 cysts in each kidney is sufficient for diagnosis. For patients aged ≥60 years, at least 4 cysts in each kidney is sufficient for diagnosis. Similarly, fewer than 2 cysts in each kidney excludes the diagnosis in at-risk patients aged ≥30 years.

Children with ADPKD are almost always asymptomatic, but adults eventually develop chronic renal insufficiency and often hypertension. The cysts of ADPKD occur in both the cortex and the medulla, are often simple, and grow over time, leading to progressive replacement of the renal parenchyma (Figure 12a-b) as well as development of renal calculi [34]. Additionally, as the cysts increase in number and size over time, the kidneys also enlarge, displacing other structures in the abdomen. ADPKD is also associated with cysts in the liver. Less commonly, cysts may also occur in the pancreas, seminal vesicles, and arachnoid membranes. Intracranial berry aneurysms are also associated with ADPKD, increasing in frequency with age.

**Acquired Cystic Kidney Disease (ACKD)—**ACKD is associated with end-stage renal disease and long-term dialysis. However, it may occur with less-advanced chronic kidney disease. It occurs due to hypertrophy of remaining functional nephrons and tubular obstruction. It is diagnosed by the presence of four or more cysts in each kidney in a patient with appropriate risk factors [35]. Typically the cysts are greater than 1 cm in size and predominately cortical in location, with intervening areas of spared renal parenchyma (Figure 12c-d). These cysts may regress after renal transplantation. Importantly, these patients have an increased risk of renal cell carcinoma (RCC), warranting close inspection to differentiate cystic from solid lesions.

**Mimic of cystic kidney disease: peripelvic cysts—**Peripelvic cysts are dilated lymphatic channels residing in the renal sinus. These channels, which have the appearance of cysts on all imaging modalities, are commonly mistaken for hydronephrosis, especially if confluent. However, when the dilation of these lymphatic channels is especially pronounced, the dilation may involve the intrarenal lymphatics as well, potentially mimicking a medullary-predominant cystic disease (Figure 13a-e).

## OTHER DISEASES

When encountering a diffuse renal process that does not predominantly feature calcifications or cysts, the differential diagnosis can be narrowed by characterizing the process as medullary-predominant, cortical-predominant, or multiple-mass-related. These entities are summarized in Figure 14.

## Medullary-predominant processes

The diseases in the medullary-predominant category include papillary necrosis and medullary ischemia, which are closely related entities.

**Papillary necrosis—**Renal papillary necrosis is characterized by ischemic necrosis of the papillary tip of the medullary pyramids [36]. The renal papillae, which receive only a marginal blood supply from the vasa recta and have a hypertonic interstitium, have an inherently increased risk for ischemic injury compared to other portions of the renal parenchyma. There is a broad array of causes for papillary necrosis which can be summarized by the POSTCARDS mnemonic (i.e., **p**yelonephritis, **o**bstruction, **s**ickle cell disease, **t**uberculosis, **c**irrhosis, **a**nalgesic / **a**lcohol abuse, **r**enal transplant rejection / **r**enal vein **t**hrombosis, **d**iabetes mellitus, **s**ystemic vasculitis). If enough papillae are involved, acute renal failure may develop.

Owing to its association with hematuria, papillary necrosis may be first encountered (and is often best depicted) on CT urography [37]. A variety of imaging features has been described (Figure 15a-c), depending on the degree of necrosis (e.g., partial or complete) and whether the papillae have sloughed off the medullary pyramid. The most commonly encountered findings include a ‘ball-on-tee’ appearance related to insinuation of concentrated contrast into the cavity left by a sloughed papilla, or a ‘lobster claw’ configuration secondary to tracking of contrast around a necrotic papilla that has not yet detached [38]. Sloughed papillae appear as rounded or triangular filling defects within a calyx or renal pelvis, though may also travel distally and cause ureteral obstruction. Occasionally, a sloughed papilla may become a nidus for calcification.

**Medullary Ischemia—**The marginal blood supply and hyperosmolar environment described above for the renal papillae applies more broadly to the entire medulla, albeit to a slightly lesser extent [36]. Ischemic changes in the medullary pyramids may be reversible if the underlying cause is corrected but may also progress to medullary infarction and papillary necrosis [39]. Notably, causes of medullary ischemia are the same as those described above in papillary necrosis (i.e., POSTCARDS mnemonic). In contradistinction to papillary necrosis, medullary ischemia is often best appreciated on CT with a nephrographic phase of contrast [39]. Imaging findings include relative hypoenhancement of the medullary pyramids with contrast pooling at the corticomedullary junctions (Figure 15d). However, many patients with medullary ischemia have no identifiable abnormality on contrast-enhanced CT.

## Cortical-predominant processes

The diseases in the medullary-predominant category include chronic kidney disease, acute pyelonephritis, and hemosiderosis.

**Chronic kidney disease—**Chronic kidney disease (CKD) is defined as a glomerular filtration rate (GFR) less than 60 ml/min/1.73 $m^2$ for a period of time greater than 3 months [40]. The most common causes include diabetes mellitus, hypertension, glomerulonephritis, and ADPKD. Renal parenchymal imaging, specifically ultrasound, often plays a role in the

management of CKD by identifying reversible causes of renal dysfunction (e.g., obstruction) and aiding in the distinction between acute kidney injury (AKI) and CKD in a patient whose baseline renal function if unknown [41]. Most causes of CKD result in parenchymal atrophy, which manifests on imaging as diffuse cortical thinning and decreased renal length (i.e., < 9 cm) (Figure 16a-b) [42]. In addition to parenchymal atrophy, sonographic findings in CKD include an increase in parenchymal echogenicity which is typically greater than the adjacent liver (assuming no coexistent hepatic steatosis) (Figure 16a-b). Additionally, the medullary pyramids become difficult to visualize and distinguish from the adjacent renal cortex. In contrast, other etiologies of CKD may be associated with diffuse renal enlargement (i.e., ADPKD).

**Acute pyelonephritis—**Acute pyelonephritis usually occurs from ascent of a lower urinary tract infection but may infrequently occur due to hematogenous spread of a concomitant infection elsewhere in the body. Imaging is not needed in the diagnosis of uncomplicated pyelonephritis as most cases can be recognized by clinical symptoms and laboratory findings. However, imaging may be performed if there is suspicion for a complication such as a renal abscess [43]. The most common sonographic abnormalities in pyelonephritis include renal enlargement, changes in renal parenchymal echogenicity, and areas of hypoperfusion on Doppler evaluation [44]. However, the majority patients with pyelonephritis (>75%) have a normal sonographic examination.

On contrast-enhanced CT, pyelonephritis is depicted by alternating areas of peripheral linear or wedge-shaped hypoenhancement and hyperenhancement, which has been termed the ‘striated nephrogram’ (Figure 16c). The striations are best appreciated in the nephrographic phase or even in the later phases. The pathophysiology underlying this imaging finding is poorly understood but may relate to areas of hyper-concentrated contrast material (i.e., hyperdense) on a background of edematous (i.e., hypodense) parenchyma [22]. Importantly, pyelonephritis is often a unilateral finding but can be bilateral in some cases. There are several other processes that present with bilateral striated nephrograms, including acute tubular necrosis, hypotension, and urine outflow obstruction (typically at the level of bladder or urethra).

**Hemosiderosis—**Renal cortical hemosiderosis occurs in the context of intravascular hemolysis, with resultant deposition of free hemosiderin in the proximal convoluted tubules. Potential etiologies include paroxysmal nocturnal hemoglobinuria, mechanical hemolysis in the setting of a prosthetic cardiac valve, sickle cell disease, and hemolytic anemia [45]. Interestingly, cortical hemosiderin deposition does not occur in the setting of primary hemochromatosis or transfusional iron overload, unless intravascular hemolysis is coexistent. Despite the degree of iron accumulation, renal function is not typically affected. Cortical hemosiderosis is only apparent on MR imaging, and findings include cortical T1-hypointensity and T2-hypointensity (Figure 17a-e) [46]. Additionally, progressive cortical signal loss occurs on gradient recalled echo (GRE) images as echo times (TEs) are lengthened.

## Multiple Masses

The differential diagnosis for multiple masses in either or both kidneys is broad and includes lymphoma, leukemia, metastatic disease, sarcoidosis, IgG4-related disease, and several tumor predisposition syndromes including Birt-Hogg-Dubé, Von Hippel-Lindau, and tuberous sclerosis (among others).

**Lymphoma—**Renal lymphoma usually occurs in conjunction with nodal and extranodal lymphomatous involvement. Primary renal lymphoma is rare [47]. Renal involvement by lymphoma is common pathologically but less commonly radiologically. There are multiple radiologic patterns of renal involvement in lymphoma, the most common of which is multiple bilateral parenchymal renal masses (Figure 18a) [48]. Other potential manifestations include diffuse renal enlargement without focal lesions, a solitary parenchymal or renal sinus mass, or perirenal soft tissue thickening. When multiple renal masses are seen in lymphoma, it is often associated with perinephric involvement, retroperitoneal lymphadenopathy, and/or splenomegaly [49]. In general, lymphomatous masses in the kidneys enhance less avidly than RCCs. These masses may distort the collecting system but do not invade it, distinguishing it from transitional cell carcinoma. MRI of the multifocal lymphomatous masses tends to show intermediate signal on T1- and T2-weighted images with significant diffusion restriction. PET performed with F-18 fluorodeoxyglucose (FDG) may show areas of active lymphoma in the kidneys, though physiologic excretion of FDG into the renal collecting system can obscure sites of disease. Renal lymphomatous involvement will often extend seamlessly from the cortex to the medulla and may also involve the renal sinus, whereas multifocal RCC tends to be cortical.

**Leukemia—**Leukemic involvement of the kidneys on autopsy series is often high, approaching 90% [50]. However, as with lymphoma, renal involvement on imaging is seen much less often observed. When renal involvement is detected, there is often other evidence of extramedullary involvement. The most common imaging manifestation is nephromegaly, which can be unilateral or bilateral. Focal areas of infiltration and enlargement may also be seen. These abnormalities tend to be geographic and/or wedge-shaped and tend to enhance less than renal parenchyma. The imaging appearance may look indistinguishable from multifocal pyelonephritis, and these imaging findings need to be correlated with laboratory analysis.

**Renal metastatic disease—**On autopsy specimens, renal metastatic disease may be seen in up to 20% of patients with metastatic cancer [51]. The incidence of renal metastatic disease detected at imaging is much lower. Among patients with solid renal masses with a known primary cancer that has metastasized, the renal lesions are more likely to be metastatic disease, especially when the renal parenchymal lesions are hypoenhancing and not clearly cortical [52, 53]. The growth rate on serial radiology studies may be rapid when compared to typical slow growth rates of primary renal neoplasms such as RCC [54]. Additionally, renal metastases may parallel the growth rate and respond to treatment observed at other sites of metastatic disease.

**Renal sarcoidosis—**Sarcoidosis is a systemic inflammatory disorder characterized pathologically by the presence of non-caseating granulomas. Renal involvement may be noted in 15-40% of patients with sarcoidosis, manifesting mostly commonly as multiple masses called sarcoidomas [55] (Figure 18b-c). When seen, these renal lesions are often accompanied by FDG-avid lymphadenopathy, potentially leading to the misdiagnosis of cancer on PET/CT [55]. A careful search for characteristic lung findings (e.g., perilymphatic nodules) can be helpful in suggesting sarcoidosis as the etiology of multiple renal masses. Additionally, patients with sarcoidosis may have nephrolithiasis and/or nephrocalcinosis (typically medullary) due to hypercalcemia resulting from vitamin D activation by granuloma macrophages. Following initiation of immunosuppression, renal sarcoidomas will often resolve, leaving behind areas of cortical scarring and volume loss.

**IgG4-related disease—**IgG4-related disease is a systemic condition in which IgG4-expressing plasma cells and lymphocytes infiltrate organs, resulting in fibrosis and tumor-like lesions. Pathologically, renal involvement manifests as tubulointerstitial nephritis [56]. The kidneys are involved in approximately 30% of patients with IgG4-related disease, usually associated with impaired renal function. On imaging, renal involvement has a nonspecific appearance, most often manifesting as multiple bilateral cortical mass-like lesions [57] (Figure 19a-e). These renal lesions may be associated with retroperitoneal fibrosis (particularly around the infrarenal aorta), which is seen in approximately 50% of cases of IgG4-related disease [49]. The appearance of autoimmune pancreatitis, a sausage-shaped pancreas with a halo of surrounding inflammation, is very helpful in suggesting IgG4-related disease as the likely etiology of multiple renal masses [58]. Biliary strictures suggesting sclerosing cholangitis can also be seen as a manifestation of IgG4-related disease in the abdomen.

**Birt-Hogg-Dubé—**Birt-Hogg-Dubé is a rare autosomal dominant inherited syndrome characterized by pulmonary cysts, oncocytic renal neoplasms, and cutaneous fibrofolliculomas (Figure 20a-b) [59]. The pulmonary cysts are often paramediastinal in location and can result in spontaneous pneumothoraces [60]. Patients often have multiple bilateral renal masses, with an increased incidence of both RCCs (particularly the chromophobe subtype), oncocytomas, and hybrid chromophobe RCC / oncocytoma tumors. These renal masses may have a range of enhancement patterns, reflecting the variety of underlying pathology subtypes [61].

**Tuberous sclerosis—**Tuberous sclerosis (TS) is a multisystem genetic disease that has multiple manifestations including adenoma sebaceum, cardiac rhabdomyoma, pulmonary lymphangioleiomyomatosis, and renal masses, most commonly angiomyolipomas (AMLs) and/or renal cysts (Figure 20c-f). Patients with TS may have a slightly increased risk of RCC [62]. These RCCs tend to occur in young patients, have a female predilection, and are often bilateral and/or multifocal [63]. AMLs often contain a mixture of macroscopic fat and soft tissue elements. However, some consist primarily of macroscopic fat, whereas others are nearly devoid of fat, giving a wide range of imaging appearances. Lipid-rich AMLs are typically straightforward to diagnose on imaging due to presence of macroscopic fat. Lipid-poor AMLs tend appear as hyperenhancing soft tissue lesions on CT, making

them difficult to differentiate from RCCs. On MRI, these lipid-poor AMLs have unique imaging features, in that they are usually T2-hypointense (like papillary RCCs) but avidly enhance (unlike papillary RCCs, which tend to enhance modestly). Additionally, lipid-poor AMLs may have intravoxel lipid (similar to clear cell RCC but distinguishable based on their characteristics on T2-weighted images). Notably, AMLs have an increased likelihood of bleeding, especially when larger than 4 cm, and hemorrhage may mask underlying fat components.

**Von Hippel-Lindau syndrome—**Von Hippel-Lindau (VHL) syndrome is an autosomal dominant genetic disease with multiorgan involvement (Figure 21a-c). Renal manifestations include including simple cysts, hyperplastic cysts, and RCCs (usually of clear cell histology). Approximately 60% of patients have renal cysts, and 24-45% have RCCs. The RCCs may be solid, cystic, or mixed solid/cystic. Lesions with *any* solid component (i.e., both solid and mixed solid/cystic lesions) are typically followed until they reach 3 cm in total diameter (i.e., including both the solid and cystic components for mixed lesions), at which point nephron-sparing techniques (e.g., enucleation, partial nephrectomy, ablation) are employed to ‘reset the clock’ and preserve native renal function for as long as possible [64-66]. Other abdominal manifestations include cystic pancreatic lesions (including true cysts, serous cystadenomas, and cystic neuroendocrine tumors) and adrenal pheochromocytomas.

## Conclusion:

Knowledge of the imaging characteristics of renal parenchymal disease will assist the radiologist in formulating appropriate differential diagnoses (Table 1). In particular, the presence or absence of calcifications, cysts, and masses – as well as their distribution with respect to the renal medulla, cortex, or both – will allow the radiologist to appropriately narrow the differential diagnosis and provide targeted recommendations for further management. Additional attention to the clinical history and extrarenal imaging findings will also allow the reader to distinguish among entities with similar imaging appearances.

## REFERENCES

1. Herts BR, Silverman SG, Hindman NM, Uzzo RG, Hartman RP, Israel GM, et al. (2017) Management of the Incidental Renal Mass on CT: A White Paper of the ACR Incidental Findings Committee. J Am Coll Radiol 15(2):2644–273.
2. Costanzo LS (2014) Renal Physiology. In: Costanzo LS (ed) Physiology. Saunders, an imprint of Elsevier Inc, Philadelphia, PA, pp. 239–302.
3. Sayer JA, Carr G, Simmons NL (2004) Nephrocalcinosis: molecular insights into calcium precipitation within the kidney. Clin Sci (Lond) 106(6):549–561. [PubMed: 15027893]
4. Wrong OM, Feest TG (1976). Nephrocalcinosis. In: Harper PS, Muir JR (eds) Advanced Medicine, 12. Pitman Medical, London, UK, pp. 394–406.
5. Yendt ER (1982) Medullary Sponge Kidney and Nephrolithiasis. N Engl J Med 306:1106–1107. [PubMed: 7070408]
6. Fabris A, Anglani F, Lupo A, Gambaro G (2013) Medullary sponge kidney: state of the art. Nephrol Dial Transplant 28(5):1111–1119. [PubMed: 23229933]

7. Koraishy FM, Ngo TTT, Israel GM, Dahl NK (2014) CT Urography for the Diagnosis of Medullary Sponge Kidney. Am J Nephrol 39:165–170. [PubMed: 24531190]
8. Hall FM (1991) Medullary sponge kidney and benign tubular ectasia. Am J Roentgenol 156(4):872–873. [PubMed: 2043208]
9. Peacock M (2002) Primary hyperparathyroidism and the kidney: biochemical and clinical spectrum. J Bone Miner Res 17 Suppl 2:N87–94. [PubMed: 12412783]
10. Fraser W (2009) Hyperparathyroidism. Lancet 374(9684):145–158. [PubMed: 19595349]
11. Buckalew VM (1989) Nephrolithiasis in renal tubular acidosis. J Urol 141(3 Pt 2):731–737. [PubMed: 2645431]
12. Vallurupalli K, Coakley KJ (2011) Case 167: alkaline-encrusted pyelitis. Radiology 258(3):954–957. [PubMed: 21339355]
13. Thoumas D, Darmallaicq C, Pfister C, Savoye-Collet C, Sibert L, Grise P, et al. (2002) Imaging characteristics of alkaline-encrusted cystitis and pyelitis. AJR Am J Roentgenol 178(2):389–392. [PubMed: 11804900]
14. Hsu CT, Wang ZJ, Yu ASL, Gould RG, Fu Y, Joe BN, et al. (2008) Physiology of renal medullary tip hyperattenuation at unenhanced CT: urinary specific gravity and the NaCl concentration gradient. Radiology 247(1):147–153. [PubMed: 18305187]
15. Lee EJ, Kim HS, Oh KS, Kim JM, Kim SM, Jung GS, et al. (1999) High Density Renal Medulla on Unenhanced CT: Significance and Relation with Hydration Status. J Korean Radiol Soc 40(3):549.
16. Tublin ME, Tessler FN, McCauley TR, Kesack CD (1997) Effect of hydration status on renal medulla attenuation on unenhanced CT scans. Am J Roentgenol 168(1):257–259. [PubMed: 8976956]
17. Matlin RA, Gary NE (1974) Acute cortical necrosis. Case report and review of the literature. Am J Med 56(1):110–118. [PubMed: 4809569]
18. Sis B, Sarioglu S, Celik A, Kasap B, Yildiz S, Kavukcu S, et al. (2006) Renal medullary changes in renal allograft recipients with raised serum creatinine. J Clin Pathol 59(4):377–381. [PubMed: 16461569]
19. Bonsib SM, Reznicek MJ, Wright FH (1989) Renal medulla in the diagnosis of acute cellular rejection. Transplantation 48(4):690–692. [PubMed: 2799925]
20. Harrison RB, Vaughan ED Jr (1978) Diffuse cortical calcification in rejected renal transplants. Radiology 126(3):635–636. [PubMed: 343167]
21. Almond PS, Matas A, Gillingham K, Dunn DL, Payne WD, Gores P, et al. (1993) Risk factors for chronic rejection in renal allograft recipients. Transplantation 55(4):752–756. [PubMed: 8475548]
22. Saunders HS, Dyer RB, Shifrin RY, Scharling ES, Bechtold RE, Zagoria RJ (1995) The CT nephrogram: implications for evaluation of urinary tract disease. Radiographics 15(5):1069–1085. [PubMed: 7501851]
23. Kuo LW, Horton K, Fishman EK (2001) CT Evaluation of Multisystem Involvement by Oxalosis. J Roentgenol 177(3):661–663.
24. Falkoff GE, Rigsby CM, Rosenfield AT (1987) Partial, combined cortical and medullary nephrocalcinosis: US and CT patterns in AIDS-associated MAI infection. Radiology 162(2):343–344. [PubMed: 3541028]
25. Gibson MS, Puckett ML, Shelly ME (2004) Renal Tuberculosis. Radiographics Jan-Feb;24(1):251–256. [PubMed: 14730050]
26. Naeem M, Zulfiqar M, Siddiqui MA, Shetty AS, Haq A, Varela C, et al. (2021) Imaging Manifestations of Genitourinary Tuberculosis. Radiographics 41(4):1123–1143. [PubMed: 34048278]
27. Dillman JR, Trout AT, Smith EA, Towbin AJ (2017) Hereditary Renal Cystic Disorders: Imaging of the Kidneys and Beyond. Radiographics 37(3):924–946. [PubMed: 28493804]
28. Wood CG, Stromberg III LJ, Harmath CB, Horowitz JM, Feng C, Hammond NA, et al. (2015) CT and MR Imaging for Evaluation of Cystic Renal Lesions and Diseases. Radiographics 35(1): 125–141. [PubMed: 25590393]

29. DiSalvo DN, Park J, Laing FC (2012) Lithium Nephropathy Unique Sonographic Findings. J Ultrasound Med 31:637–644. [PubMed: 22441921]
30. Oliva MR, Hsing J, Rybicki FJ, Fennessy F, Mortelé KJ, Ros PR (2003) Glomerulocystic kidney disease: MRI findings. Abdom Imaging 28:889–892. [PubMed: 14753613]
31. Garel LA, Habib R, Pariente D, Broyer M, Sauvegrain J (1984) Juvenile nephronophthisis: sonographic appearance in children with severe uremia. Radiology 151(1):93–95. [PubMed: 6701346]
32. Lonergan GJ, Rice RR, Suarez ES (2000) Autosomal recessive polycystic kidney disease: radiologic-pathologic correlation. Radiographics 20(3):837–855. [PubMed: 10835131]
33. Mufti WB, Nalagatla SK (2010) Nephrolithiasis in autosomal dominant polycystic kidney disease. J Endourol 24(10):1557–1561. [PubMed: 20818989]
34. Pei Y, Obaji J, Dupuis A, Paterson AD, Magistroni R, Dicks E, et al. (2009) Unified Criteria for Ultrasonographic Diagnosis of ADPKD. J Am Soc Nephrol 20(1):205–212. [PubMed: 18945943]
35. Choyke PL (2000) Acquired cystic kidney disease. Eur Radiol 10(11):1716–1721. [PubMed: 11097395]
36. Jung DC, Kim SH, Jung SI, Hwang SI, Kim SH (2006) Renal Papillary Necrosis: Review and Comparison of Findings at Multi–Detector Row CT and Intravenous Urography. RadioGraphics 26(6):1827–1836. [PubMed: 17102053]
37. Kawamoto S, Duggan P, Sheth S, Miyamoto H, Kazi ZN, Fishman EK (2017) Renal Papillary and Calyceal Lesions at CT Urography: Genitourinary Imaging. RadioGraphics 37(1):358–359. [PubMed: 28076022]
38. Dyer RB, DiSantis DJ (2014) The golf ball-on-tee sign. Abdom Imaging 39(6):1356–1357. [PubMed: 25173792]
39. Lang EK, Macchia RJ, Thomas R, Davis R, Ruiz-Deya G, Watson RA, et al. (2003) Detection of medullary and papillary necrosis at an early stage by multiphasic helical computerized tomography. J Urol 170(1):94–98. [PubMed: 12796654]
40. Eknoyan G, Lameire N, Eckardt K, Kasiske BL, Wheeler DC, Abboud OI, et al. (2013) KDIGO 2012 clinical practice guideline for the evaluation and management of chronic kidney disease. Kidney Int 3(1):5–14.
41. Faubel S, Patel NU, Lockhart ME, Cadnapaphornchai MA (2014) Renal Relevant Radiology: Use of Ultrasonography in Patients with AKI. Clin J Am Soc Nephrol 9(2):382–394. [PubMed: 24235286]
42. Beland MD, Walle NL, Machan JT, Cronan JJ (2010) Renal Cortical Thickness Measured at Ultrasound: Is It Better Than Renal Length as an Indicator of Renal Function in Chronic Kidney Disease? Am J Roentgenol 195(2):W146–149. [PubMed: 20651174]
43. Nikolaidis P, Dogra VS, Goldfarb S, Gore JL, Harvin HJ, Heilbrun ME, et al. (2018) ACR appropriateness criteria® acute pyelonephritis. J Am Coll Radiol 15(11):S232–239. [PubMed: 30392592]
44. Craig WD, Wagner BJ, Travis MD (2008) Pyelonephritis: radiologic-pathologic review. Radiogr Rev Publ Radiol Soc N Am Inc 28(1):255–277; quiz 327–328.
45. Queiroz-Andrade M, Blasbalg R, Ortega CD, Rodstein MAM, Baroni RH, Rocha MS, et al. (2009) MR Imaging Findings of Iron Overload. RadioGraphics 29(6):1575–1589. [PubMed: 19959509]
46. Jeong JY, Kim SH, Lee HJ, Sim JS (2002) Atypical Low-Signal-Intensity Renal Parenchyma: Causes and Patterns. RadioGraphics 22(4):833–846. [PubMed: 12110713]
47. Ganeshan D, Iyer R, Devine C, Bhosale P, Paulson E (2013) Imaging of Primary and Secondary Renal Lymphoma. AJR 201:W712–W719. [PubMed: 24147501]
48. Sheth S, Ali S, Fishman E (2006) Imaging of renal lymphoma: patterns of disease with pathologic correlation. RadioGraphics 26(4):1151–1168. [PubMed: 16844939]
49. Purysko A, Westphalen A, Remer E, Coppa CP, Filho HML, Herts BR (2016) Imaging Manifestations of Hematologic Diseases with Renal and Perinephric Involvement. RadioGraphics 36:1038–1054. [PubMed: 27257766]
50. Bach AG, Behrmann C, Holzhausen HJ, Katzer M, Arnold D, Spielmann RP, et al. (2012) Prevalence and patterns of renal involvement in imaging of malignant lymphoproliferative diseases. Acta Radiol 53(3):343–348. [PubMed: 22287149]

51. Choyke PL, White EM, Zeman RK, Jaffe MH, Clark LR (1987) Renal metastases: clinicopathologic and radiologic correlation. Radiology 162(2):359–363. [PubMed: 3797648]
52. Sanchez-Ortiz R, Madsen L, Bermejo C, Wen S, Shen Y, Swanson DA, et al. (2004) A Renal Mass in the Setting of a Nonrenal Malignancy. Cancer 101(10):2195–2201. [PubMed: 15470708]
53. Patel U, Ramachandran N, Halls J, Parthipun A, Slide C (2011) Synchronous Renal Masses in Patients With a Nonrenal Malignancy: Incidence of Metastasis to the Kidney Versus Primary Renal Neoplasia and Differentiating Features on CT. AJR 197:W680–W686. [PubMed: 21940540]
54. Chawla SN, Crispen PL, Hanlon AL, Greenberg RE, Chen DYT, Uzzo RG (2006) The natural history of observed enhancing renal masses: meta-analysis and review of the world literature. J Urol 175(2):425–431. [PubMed: 16406965]
55. Correia F, Marchini G, Torricelli F, Danilovic A, Vicentini FC, Srougi M, et al. (2020) Renal manifestations of sarcoidosis: from accurate diagnosis to specific treatment. Int Braz J Urol 46(1):15–25. [PubMed: 31851454]
56. Cornell LD (2012) IgG4-related kidney disease. Semin Diagn Pathol 29(4):245–250. [PubMed: 23068304]
57. Capecchi R, Giannese D, Moriconi D, Bonadio AG, Pratesi F, Croia C, et al. (2021) Renal Involvement in IgG4-Related Disease: From Sunlight to Twilight. Frontiers in Medicine 1–10.
58. Martínez-de-Alegría A, Baleato-González S, García-Figueiras R, Bermúdez-Naveira A, Abdulkader-Nallib I, Díaz-Peromingo JA, et al. (2015) IgG4-related Disease from Head to Toe. RadioGraphics 35(7):2007–2025. [PubMed: 26473450]
59. Zamora CA, Rowe S, Horton KM (2015) Case 218: Birt-Hogg-Dube Syndrome. Radiology 275(3): Vol 275:Number 3.
60. Gupta N, Kpras E, Henske E, James LE, El-Chemaly S, Veeraraghavan S, et al. (2017) Spontaneous Pneumothoraces in Patients with Birt–Hogg–Dubé Syndrome. Annals of the American Thoracic Society 14(5):706–713. [PubMed: 28248571]
61. Gupta S, Kang H, Ganeshan D, Morani A, Gautam R, Choyke PL, et al. (2017) The ABCs of BHD: An In-Depth Review of Birt-Hogg-Dube Syndrome. AJR 209:1291–1296. [PubMed: 28981362]
62. Von Ranke F, Zanetti G, e Silva J, Neto CAA, Godoy MCB, Souza CA, et al. (2015) Tuberous Sclerosis Complex: State-of-the-Art Review with a Focus on Pulmonary Involvement. Lung 193(95):619–627. [PubMed: 26104489]
63. Umeoka S, Koyama T, Miki Y, Akai M, Tsutsui K, Togashi K (2008) Pictorial review of tuberous sclerosis in various organs. Radiographics 28(7):e32. [PubMed: 18772274]
64. Leung RS, Biswas SV, Duncan M, Rankin S (2008) Imaging Features of von Hippel–Lindau Disease. RadioGraphics 28:65–79. [PubMed: 18203931]
65. Ganeshan D, Menias CO, Pickhardt PJ, Sandrasegaran K, Lubner MG, Ramalingam P, et al. (2018) Tumors in von Hippel-Lindau Syndrome: From Head to Toe-Comprehensive State-of-the-Art Review. RadioGraphics 38:849–866. [PubMed: 29601266]
66. Ploussard G, Droupy S, Ferlicot S, Ples R, Rocher L, Richard S, et al. (2007) Local Recurrence After Nephron-Sparing Surgery in von Hippel-Lindau disease. Urology 7;70(3):435–439.

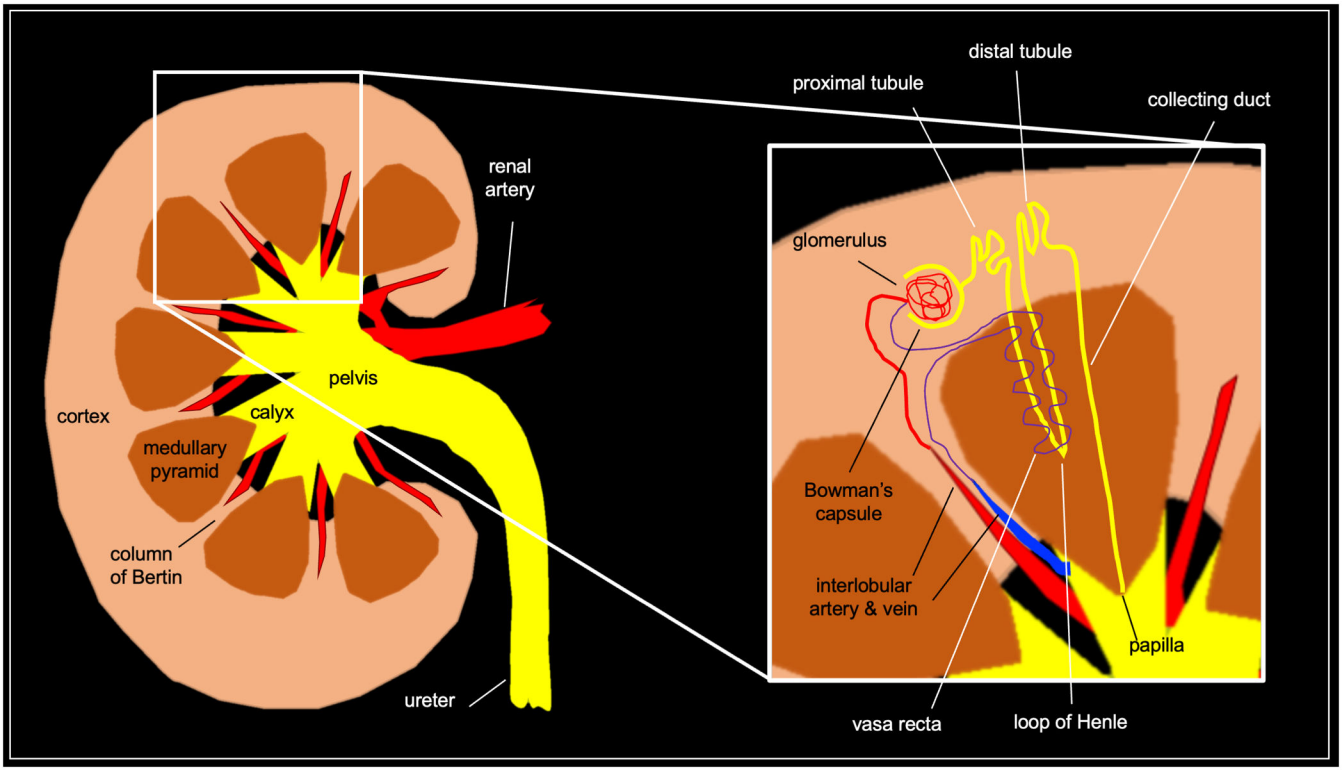


**Fig 1. Gross and microscopic renal anatomy.**

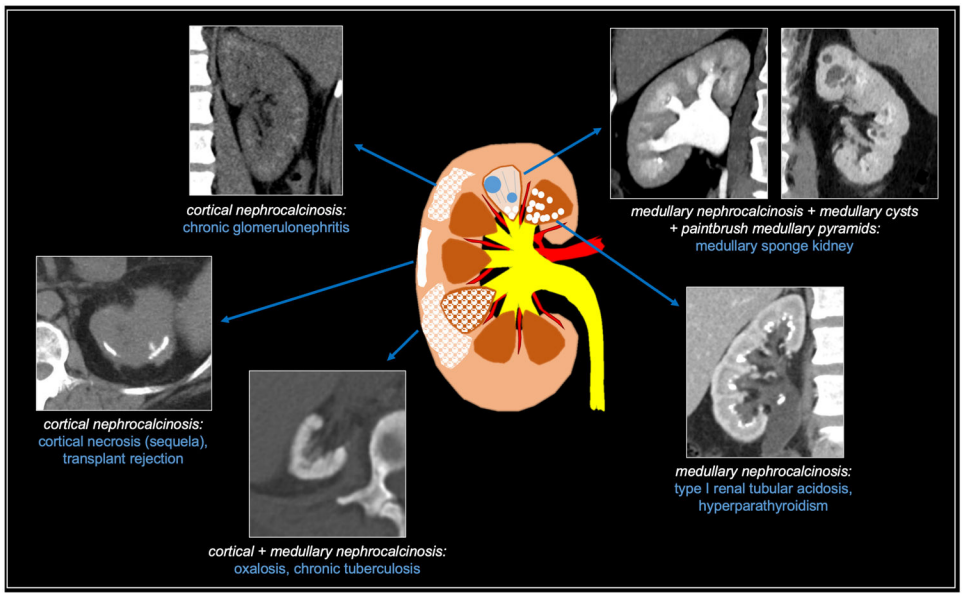


**Fig 2. Summary of calcific diffuse renal diseases.**

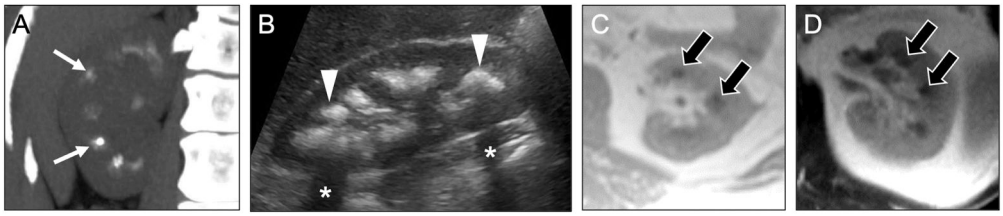


**Fig 3. Imaging appearances of medullary nephrocalcinosis.**

Coronal maximum intensity projection image from noncontrast CT (**a**) and longitudinal image from sonogram (**b**) in a 35-year-old woman show hyperdensity (arrows) and hyperechogenicity (arrowheads) with shadowing (asterisks), consistent with medullary nephrocalcinosis. Axial T1-weighted (**c**) and T2-weighted (**d**) MR images in a 47-year-old women with known medullary nephrocalcinosis show hypointensity (black arrows) of the medullary pyramids due to susceptibility-related signal loss from dense calcification.

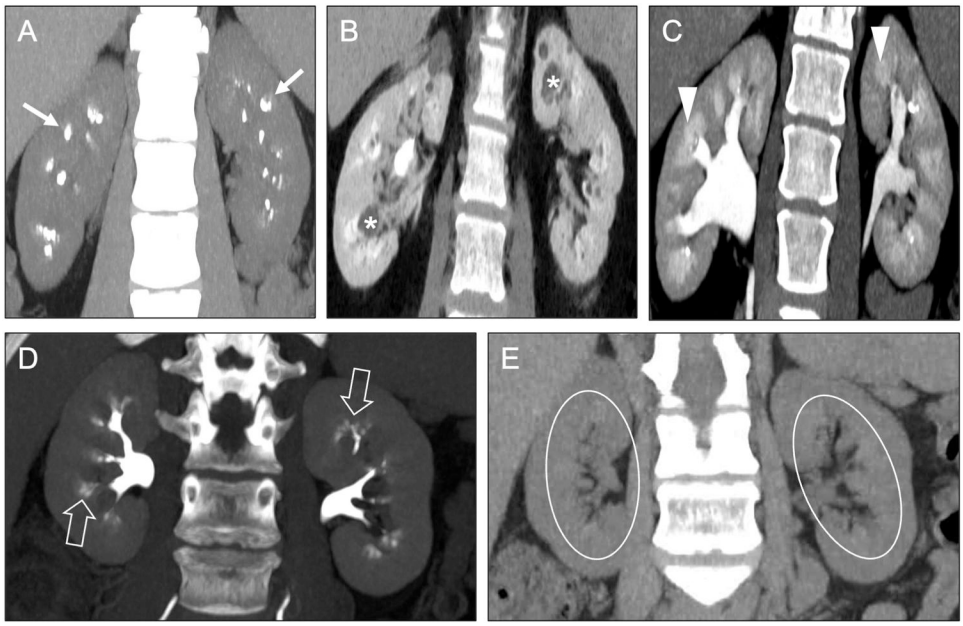


**Fig 4. Medullary sponge kidney versus tubular ectasia.**

Coronal noncontrast (**a**) and contrast-enhanced CT images in the nephrographic (**b**) and urographic (**c**) phases in a 44-year-old woman show dense medullary calcifications (arrows), medullary-predominant cysts (asterisks), and ‘paintbrush’ appearance (arrowheads) of the medullary pyramids. This constellation of findings is consistent with medullary nephrocalcinosis secondary to medullary sponge kidney. In contrast, coronal contrast-enhanced urographic phase (**d**) and noncontrast (**e**) CT images in a 65-year-old woman with tubular ectasia show dilated collecting ducts in the medullary pyramids (open arrows), also creating a ‘paintbrush’ appearance, but without associated medullary nephrocalcinosis (ovals).

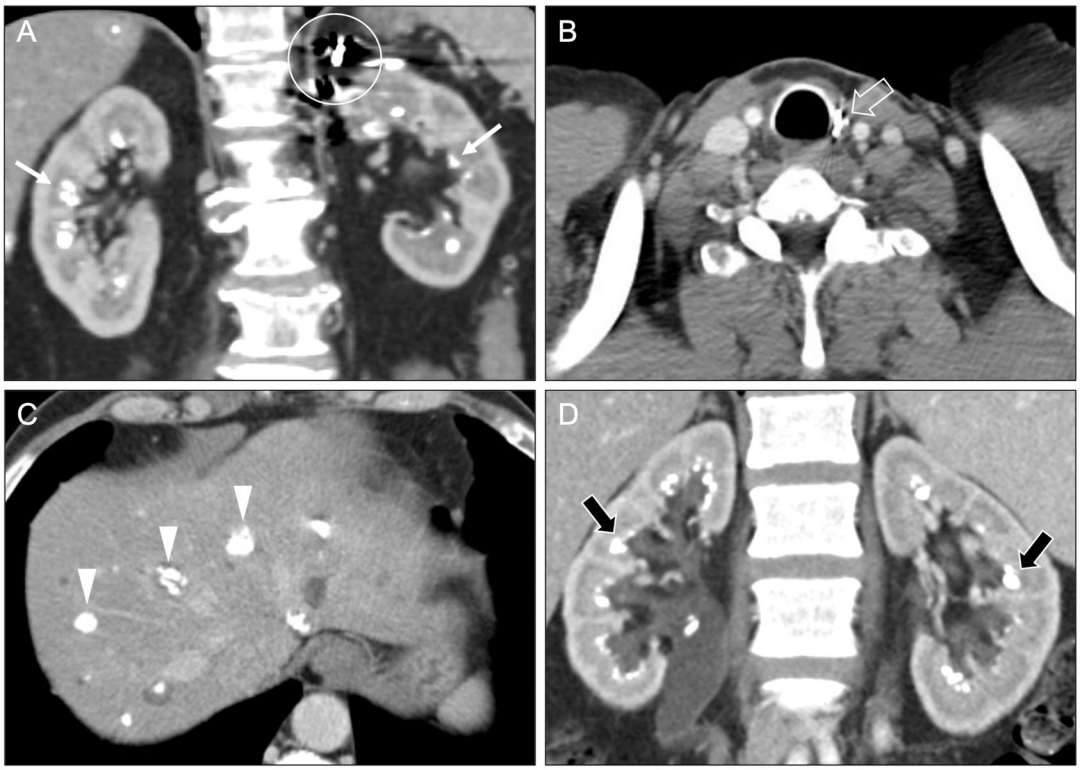


**Fig 5. Other causes of medullary nephrocalcinosis.**

Coronal (**a**) and axial (**b**, **c**) contrast-enhanced CT images in a 61-year-old man with MEN 2A syndrome show medullary nephrocalcinosis (arrows) related to a hypercalcemia from a prior parathyroid adenoma. Surgical clips from prior left adrenalectomy (circle) and thyroidectomy (open arrow) relate to prior resections of pheochromocytoma and medullary thyroid carcinoma, respectively. Calcified hepatic lesions (arrowheads) represented medullary thyroid carcinoma metastases. Coronal contrast-enhanced CT images (**d**) in a 43-year-old woman with type 1 renal tubular acidosis show symmetric bilateral medullary nephrocalcinosis (black arrows).

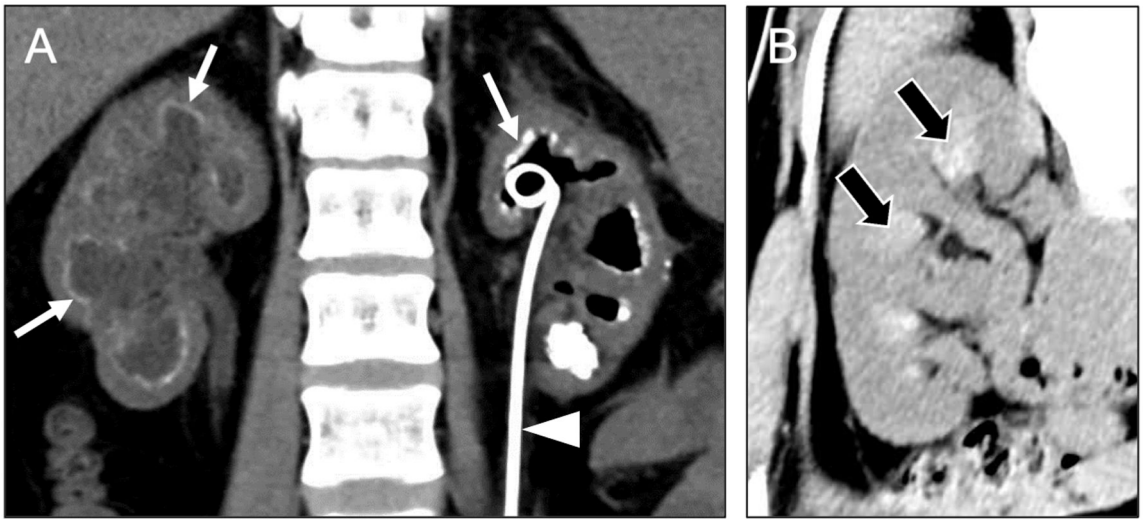


**Fig 6. Mimics of medullary nephrocalcinosis.**

Coronal noncontrast CT image (**a**) in a 40-year-old woman with alkaline-encrusted pyelitis shows dilated collecting systems with coating of the urothelium by a thin layer of calcification (arrows) and a left ureteral stent in place (arrowhead). Coronal noncontrast CT image (**b**) in a 36-year-old woman with acute dehydration shows hyperdensity of the medullary pyramids (black arrows). Finding resolved in subsequent examinations after treatment.

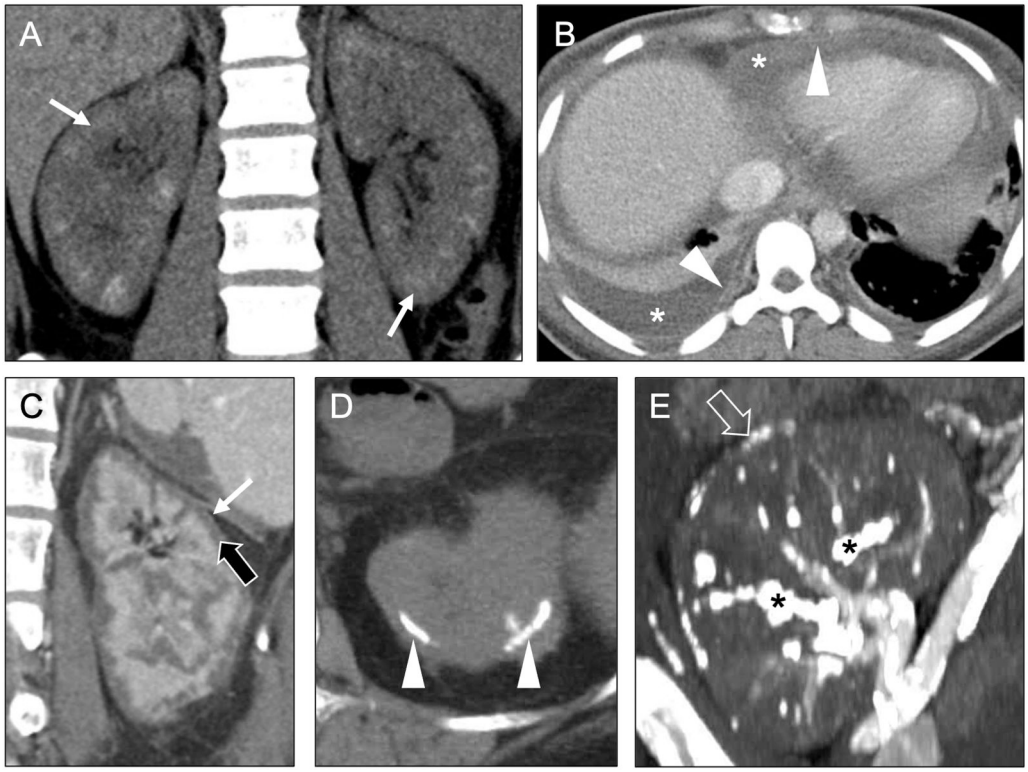


**Fig 7. Causes of cortical nephrocalcinosis.**

Coronal noncontrast (**a**) and axial contrast-enhanced (**b**) CT images in a 25-year-old woman reveal ill-defined calcifications in the renal cortex (arrows) compatible with cortical nephrocalcinosis, as well as pericardial and pleural effusions (asterisks) with serosal enhancement (arrowheads) indicating active pleuritis and pericarditis. These findings of active pleuritis and pericarditis are consistent with lupus-related chronic glomerulonephritis as the etiology of the patient's cortical nephrocalcinosis. Coronal contrast-enhanced CT image (**c**) in a 33-year-old man presenting with systemic hypotension secondary to a gunshot wound shows diffuse cortical hypoenhancement (black arrow) with a thin rim of hyperenhancement along the renal capsule (white arrow), also known as the 'cortical rim sign.' Axial noncontrast CT image (**d**) from a subsequent examination in the same patient shows dense cortical calcification (arrowheads), indicating cortical nephrocalcinosis related to the prior episode of acute cortical necrosis. Finally, a coronal noncontrast CT image (**e**) in a 66-year-old man with chronic rejection of a now non-functioning renal transplant shows dense cortical calcifications (open arrow), as well as extensive vascular calcifications (asterisk).

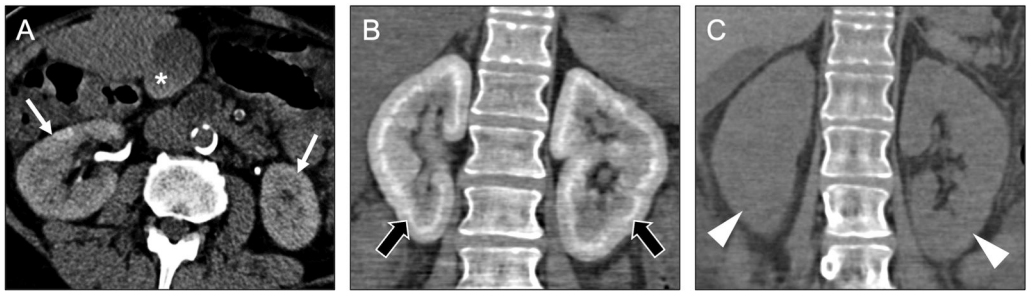


**Fig 8. Mimics of cortical nephrocalcinosis.**

Axial noncontrast CT image (**a**) in a 55-year-old man who had undergone a contrast-enhanced CT several days prior shows cortical-predominant retention of contrast medium in both kidneys (arrows), consistent with acute tubular necrosis. Vicarious excretion of contrast material via the biliary system (asterisk) may provide an additional clue to this diagnosis in less clear-cut cases. Coronal noncontrast CT image (**b**) in a 67-year-old man with acute renal failure shows hyperdensity throughout the renal cortices (black arrows), a finding initially misinterpreted as cortical nephrocalcinosis. A follow-up CT (**c**) in the same patient shows resolution of the hyperdensity (arrowheads), confirming that this finding instead represented retained contrast material in the setting of acute tubular necrosis.

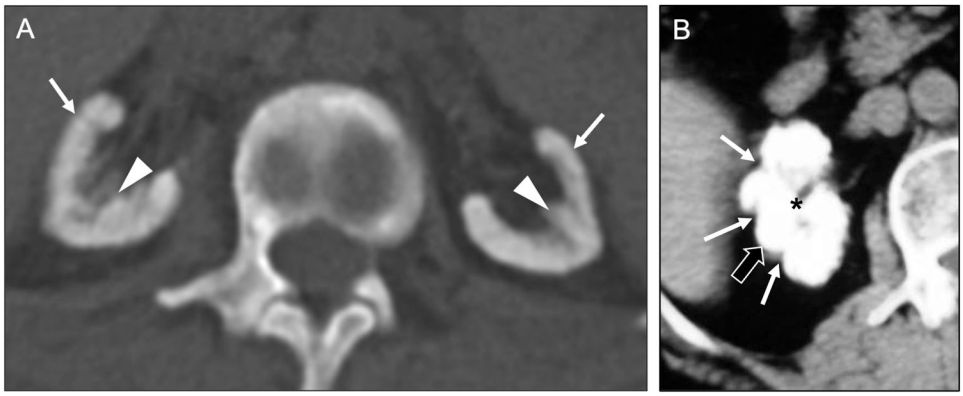


**Fig 9. Causes of combined cortical and medullary nephrocalcinosis.**

Axial noncontrast CT image (**a**) in a 34-year-old woman with primary oxalosis show diffuse hyperdensity throughout the cortex (arrows) and medulla (arrowheads) of both kidneys. The kidneys are atrophic but otherwise normal in morphology. A axial noncontrast CT image (**b**) in a patient with chronic renal failure and history of tuberculosis shows an atrophic kidney with dense calcification throughout the cortex (black arrow) and medulla (asterisk) with extensive cortical scarring (white arrows), consistent with a ‘putty kidney’ from prior tuberculous involvement.

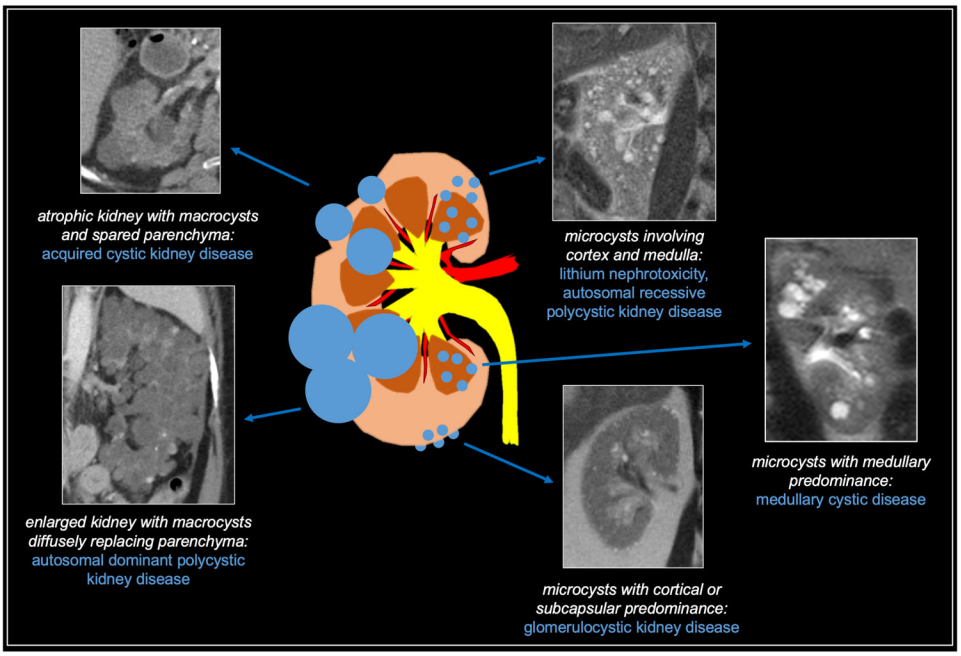


**Fig 10. Summary of cystic diffuse renal diseases.**

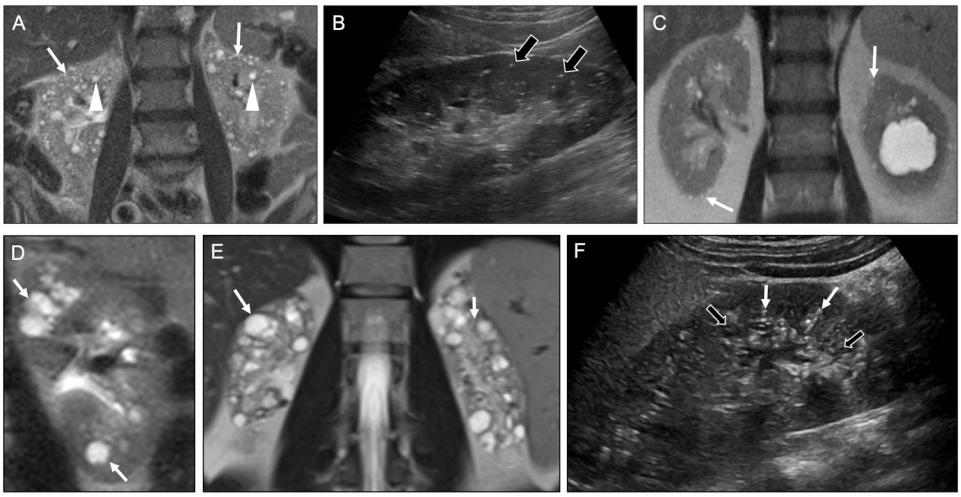


**Fig 11. Causes of microcystic diffuse renal disease.**

Coronal T2-weighted MR image (**a**) in a 74-year-old woman with history of psychiatric disease show numerous predominantly subcentimeter cysts throughout the cortex (arrows) and medulla (arrowheads). These findings are consistent with lithium nephrotoxicity. Longitudinal sonographic image (**b**) in a 76-year-old man with history of lithium use shows multiple punctate echogenic foci without shadowing (black arrows), consistent with microcysts from lithium nephrotoxicity. Note that tiny cysts often appear echogenic rather than anechoic on ultrasound. In contrast, a coronal T2-weighted MR image (**c**) in an 82-year-old man with chronic kidney disease shows microcysts with a cortical and subcapsular predominance (arrows), an appearance characteristic of glomerulocystic kidney disease. Coronal T2-weighted MR image (**d**) in 12-year-old girl shows cysts isolated to the renal medulla (white arrows), a characteristic appearance of medullary cystic renal disease. Coronal T2-weighted MR image (**e**) in a 29-year-old man with autosomal recessive polycystic kidney disease shows bilateral atrophic kidneys that are replaced by innumerable cysts. Longitudinal sonographic image (**f**) in a 20-year-old woman with autosomal recessive polycystic kidney disease shows an enlarged kidney with multiple small echogenic (white arrows) and anechoic (black arrows) cysts. As with lithium nephrotoxicity, tiny cysts may appear echogenic rather than anechoic.

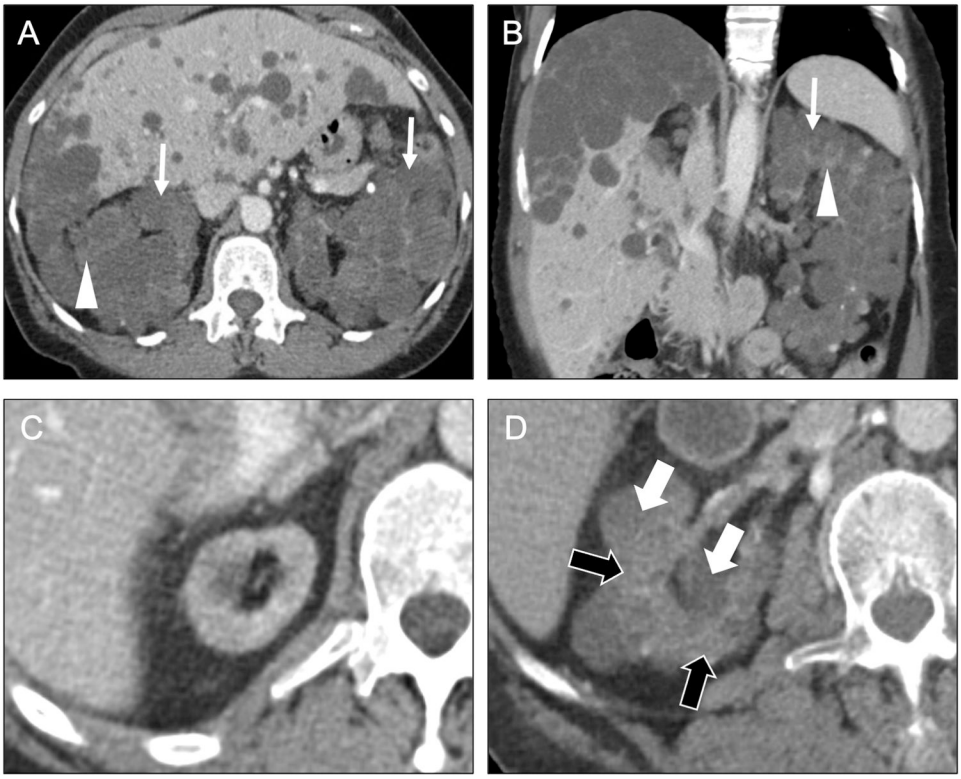


**Fig 12. Causes of macrocystic diffuse renal disease.**

Axial (**a**) and coronal (**b**) contrast-enhanced CT images in a 61-year-old man with end-stage renal disease enlarged kidneys with near complete replacement of normal parenchyma (arrowheads) by numerous cysts (arrows). The cysts are mostly greater than 1 cm in diameter. Additionally, numerous cysts are seen in the liver. These findings are consistent with autosomal dominant polycystic disease. Axial contrast-enhanced CT images (**c**, **d**) in a 65-year-old man with end-stage renal disease on hemodialysis (10-year interval from **c** to **d**) show development of multiple macrocysts (white arrows) within the right kidney, with areas of spared renal parenchyma (black arrows) between the cysts. The kidney is also atrophic. These imaging findings in a patient with chronic kidney disease are consistent with acquired cystic kidney disease.

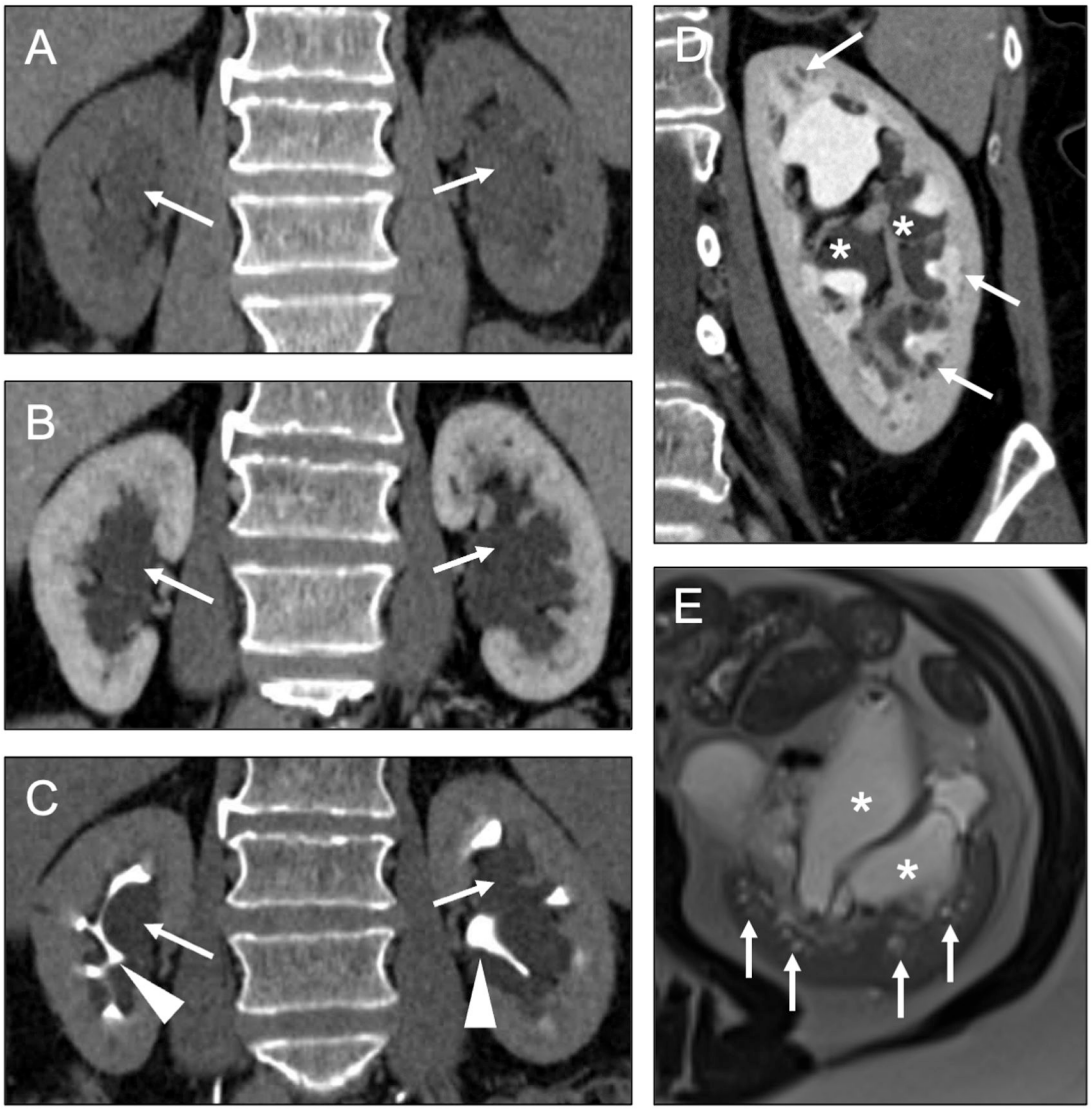


**Fig 13. Mimic of cystic diffuse renal disease.**

Coronal noncontrast (**a**) and contrast-enhanced CT images in the nephrographic (**b**) and excretory (**c**) phases in a 78-year-old man show fluid-density structures (arrows) in the renal hila. This imaging finding might be confused with hydronephrosis. However, excretory phase images show that these structures do not communicate with the renal collecting systems (arrowheads). These hilar structures are consistent with peripelvic cysts, which are dilated renal sinus lymphatic channels. Coronal contrast-enhanced excretory phase CT (**d**) and axial T2-weighted MR (**e**) images in a 56-year-old woman show extension of the dilated renal sinus lymphatics (asterisks) into the renal medulla (arrows), highlighting the potential for this entity to be confused for a cystic diffuse renal disease.

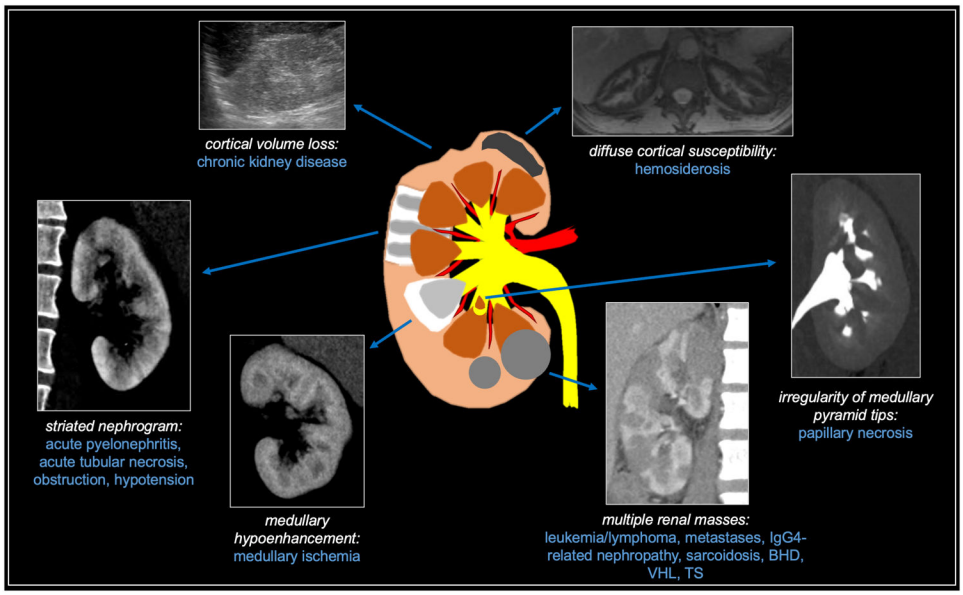


**Fig 14. Summary of other diffuse renal diseases.**

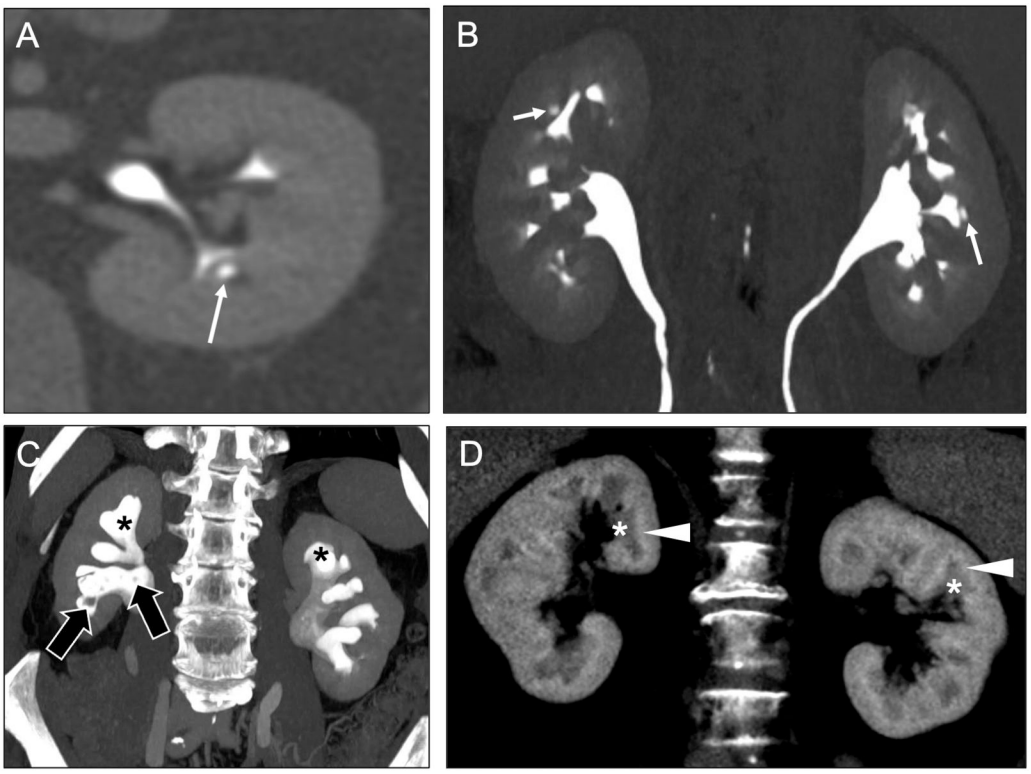


**Fig 15. Other diffuse renal diseases with medullary predominance.**

Axial contrast-enhanced CT image in the excretory phase (**a**) in a 73-year-old man with hematuria and history of sickle cell disease shows irregularity of a renal papilla, with central contrast pooling (arrow), consistent with the 'ball-on-tee' appearance of papillary necrosis. This diffuse nature of the papillary necrosis (arrows) is shown to advantage on a coronal maximum intensity projection (MIP) image (**b**) from this same CT examination. In an 86-year-old man with more advanced papillary necrosis, a coronal MIP image from a contrast-enhanced CT in the excretory phase (**c**) shows sloughed papillae (black arrows) in the collecting system, resulting in a blunted appearance of the calyces (asterisks). Coronal contrast-enhanced CT image (**d**) in a 59-year-old man shows hypoenhancement of the medullary pyramids (asterisks) and contrast pooling at the corticomedullary junctions (arrowheads). These findings are consistent with medullary ischemia and can lead to papillary necrosis if the inciting factor is not identified and corrected.

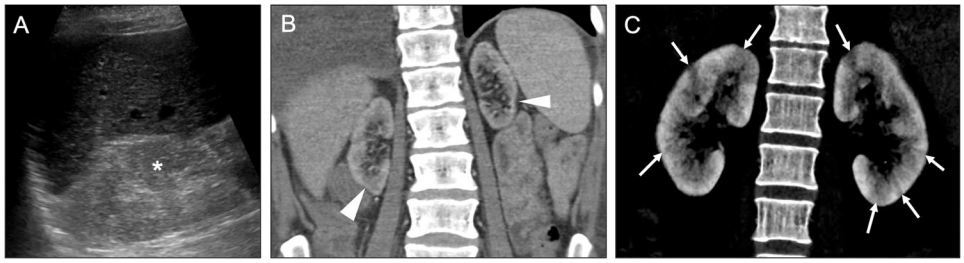


**Fig 16. Other diffuse renal diseases with cortical predominance.**

Axial sonographic (**a**) and coronal contrast-enhanced (**b**) CT images in a 50-year-old woman with creatinine value elevated show hyperechogenicity of the right kidney relative to the liver with loss of corticomedullary differentiation (asterisk), as well as small renal size and focal areas of cortical thinning (arrowheads). These findings indicated chronic kidney disease, rather than simply acute renal failure, as the cause for her elevated creatinine. Coronal contrast-enhanced CT image (**c**) in a 36-year-old man with fever shows striated nephrograms due to patchy linear areas of cortical hypoenhancement (arrows). There is a differential for bilateral striated nephrograms, but the clinical history suggested pyelonephritis.

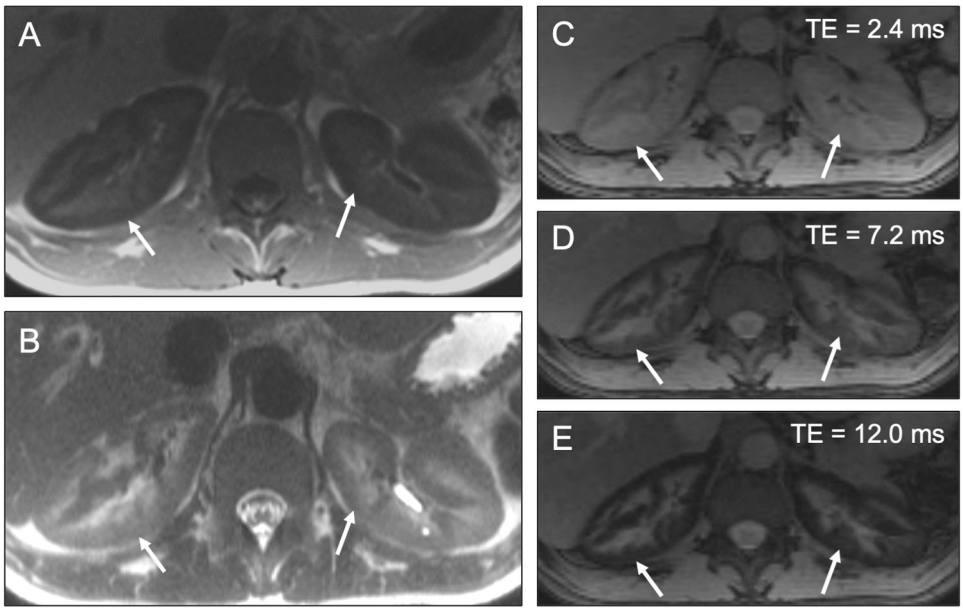


**Fig 17. Diffuse cortical signal abnormality in patient with renal hemosiderosis.**

Axial T1-weighted (**a**) and T2-weighted (**b**) MR images in a 32-year-old man show unexpectedly low signal throughout the renal cortices (arrows) with sparing of the medulla. Axial multiecho Dixon images (**c-e**) show progressive signal loss in the renal cortex (arrows) with longer echo times (TEs), confirming renal cortical iron deposition and suggesting an etiology of intravascular hemolysis. This patient had sickle cell disease.

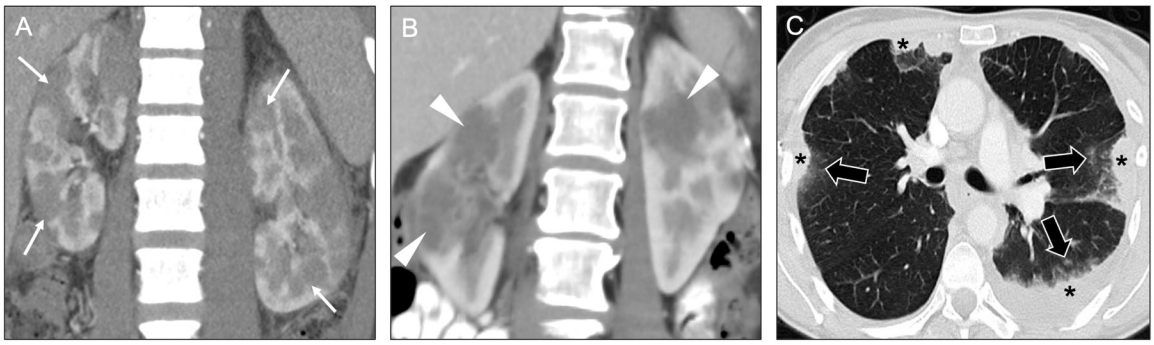


**Fig 18. Utility of clinical history and secondary findings for diagnosing diffuse renal diseases presenting as multiple masses.**

Coronal contrast-enhanced CT image (**a**) in a 34-year-old man with known lymphoma shows multiple hypoenhancing masses (arrows) in both kidneys. The presence of lymphadenopathy above and below the diaphragm (not shown) pointed to lymphomatous involvement of the kidneys as the most likely etiology of the renal masses. Coronal contrast-enhanced CT image (**b**) in a 58-year-old woman with sarcoidosis shows multiple bilateral hypoenhancing renal masses (arrowheads). Concurrently acquired axial CT image from the lungs (**c**) shows multiple areas of consolidation (asterisks), some of which were surrounding by small satellite nodules (black arrows), strongly suggesting granulomatous inflammation. In this case, the lung findings help narrow the differential for the renal lesions. The renal lesions resolved with immunosuppression (not shown).


**Fig 19. Multiple renal masses in a patient with IgG4-related disease.**

In a 60-year-old man with recent episode of pancreatitis, axial contrast-enhanced T1-weighted (**a**) and axial diffusion-weighted (**b**) MR images with ADC map (**c**) show multiple hypoenhancing, diffusion-restricting bilateral renal masses, which carry a wide differential. Axial contrast-enhanced T1-weighted (**d**, **f**) and coronal T2-weighted (**e**) MR images show an enhancing rind of soft tissue around the pancreas (black arrows) and abdominal aorta (arrowheads), as well as biliary strictures at the hepatic hilum (white arrow). This constellation of findings is consistent with IgG4 disease, making it likely that the renal masses are a manifestation of tubulointerstitial nephritis.

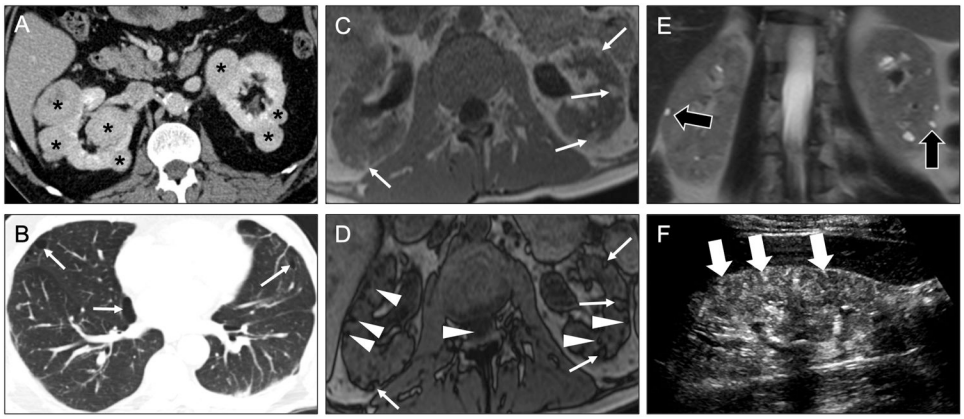


**Fig 20. Multiple renal masses in patients with Birt-Hogg-Dubé syndrome and tuberous sclerosis.**

Axial contrast-enhanced CT images of the abdomen (**a**) and chest (**b**) in a 76-year-old man show multiple bilateral renal masses (asterisks); coexisting basilar-predominant pulmonary cysts, some of which are paramediastinal in location, point to a diagnosis of Birt-Hogg-Dubé syndrome. In a 45-year-old man (**c**-**f**), axial in-phase (**c**) and opposed-phase (**d**) T1-weighted MR images show multiple small renal masses (arrows) that are isointense to the adjacent retroperitoneal fat with surrounding India ink artifact on the opposed-phase image. These lesions are consistent with angiomyolipomas (AMLs). Note that additional small foci of signal loss on the opposed-phase images (arrowheads) correspond to additional tiny AMLs that were harder to appreciate on the in-phase images due to their cortical location. Coronal T2-weighted MR image (**e**) show small renal cysts (black arrows), a typical coexisting finding in tuberous sclerosis. Longitudinal sonographic image (**f**) shows numerous small echogenic renal lesions (white arrows), corresponding to the AMLs seen on MRI.

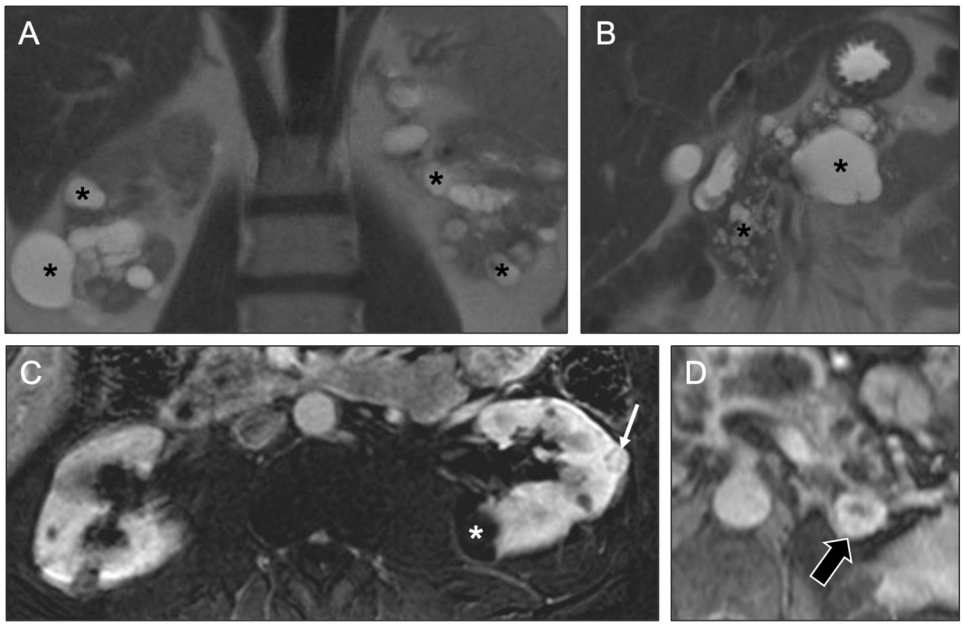


**Fig 21. Multiple renal masses in a patient with Von Hippel-Lindau syndrome.**

Coronal T2-weighted MR images (**a**, **b**) in a 58-year-old man show multiple cysts (asterisks) of varying sizes throughout the kidneys and pancreas. Axial subtracted contrast-enhanced T1-weighted MR image of the kidneys in the nephrographic phase (**c**) shows small enhancing renal masses (arrow), in addition in the nonenhancing cysts (asterisk), likely a renal cell carcinoma. This constellation of findings strongly suggests Von Hippel-Lindau (VHL) syndrome. Axial contrast-enhanced T1-weighted MR image of the left adrenal gland showed an enhancing nodule (black arrow) was concerning for a pheochromocytoma in light of the suspected VHL.

**Table 1.**

Key clinical/imaging features of diffuse renal diseases.

| | |
|---|---|
| **CALCIFIC** | |
| **Medullary nephrocalcinosis** | |
| Medullary sponge kidney | Potentially asymmetric/segmental medullary $Ca^{2+}$, medullary-predominant cysts, 'paintbrush' medullary pyramids |
| Hypercalcemia (hyperparathyroidism) | Symmetric medullary $Ca^{2+}$; look for rugger jersey spine, brown tumors, etc.; possible MEN syndrome association |
| Hypercalcemia (sarcoidosis) | Symmetric medullary $Ca^{2+}$; look for renal masses, LAD, perilymphatic pulmonary nodules |
| Distal renal tubular acidosis | Symmetric medullary $Ca^{2+}$; evidence of systemic acidosis on labs; associated with autoimmune diseases |
| *Mimic: alkaline-encrusted pyelitis* | $Ca^{2+}$lining urothelial surfaces of renal pelvis/calyces; debilitated patients with urologic interventions |
| *Mimic: dehydration* | Ill-defined hyperdensity; rapidly develops and resolves with treatment |
| **Cortical nephrocalcinosis** | |
| Chronic glomerulonephritis | Patchy or diffuse cortical $Ca^{2+}$, potentially ill-defined; look for associated findings to suggest GPA, SLE, etc. |
| Acute tubular necrosis (sequela) | Atrophy with variable cortical $Ca^{2+}$ pattern with atrophy; history of severe hypotension |
| Renal transplant rejection | Dense cortical $Ca^{2+}$, potentially patchy; clinical history of failed renal transplant |
| *Mimic: acute tubular necrosis* | Diffuse cortical hyperdensity on noncontrast CT following prior contrast study; look for vicarious biliary excretion |
| **Cortical + medullary nephrocalcinosis** | |
| Oxalosis | Bilateral cortical and medullary $Ca^{2+}$; renal atrophy without scarring |
| Tuberculosis infection (sequela) | Usually unilateral (sometimes bilateral) cortical and medullary $Ca^{2+}$; renal atrophy with scarring |
| **CYSTIC** | |
| **Microcystic** | |
| Lithium nephrotoxicity | Numerous subcentimeter cysts throughout cortex and medulla; history of psychiatric disease |
| Glomerulocystic kidney disease | Multiple subcentimeter cysts with cortical / subcapsular predominance |
| Medullary cystic disease | Multiple mostly subcentimeter cysts (though can be larger) with medullary predominance |
| ARPKD | Enlarged kidneys; cysts often not apparent on imaging; may see cortical/medullary cysts, mostly subcentimeter |
| **Macrocystic** | |
| ADPKD | Numerous > 1 cm cortical/medullary cysts replacing normal parenchyma; renal enlargement |
| Acquired cystic kidney disease | Numerous > 1 cm cortical/medullary cysts with areas of parenchymal sparing; renal atrophy |
| *Mimic: peripelvic cysts* | Multiple cystic lesions in renal hilum, not communicating with collecting system; may extend into medulla |
| **OTHER** | |

*Abdom Radiol (NY)*. Author manuscript; available in PMC 2023 July 01.

| | |
|---|---|
| **CALCIFIC** | |
| **Medullary-predominant** | |
| Medullary ischemia | Hypoenhancement of medullary pyramids with contrast pooling at corticomedullar junctions |
| Papillary necrosis | Irregularity of papillae with contrast insinuation; sloughed papillae in collecting system; history of hematuria |
| **Cortical-predominant** | |
| Acute pyelonephritis | Linear segmental cortical hypoenhancement; differential includes hypotension, obstruction, ATN if bilateral |
| Chronic kidney disease | Loss of corticomedullary differentiation; cortical thinning with scarring; small renal size |
| Hemosiderosis | Hypointensity of renal cortices from intravascular hemolysis; may coexist with secondary hemosiderosis |
| **Multiple solid masses** | |
| Leukemia/lymphoma | Most commonly multiple solid masses (lymphoma) or diffuse enlargement (leukemia); look for splenomegaly, LAD |
| Metastases | Multiple solid renal masses; look for primary malignancy elsewhere and/or history of cancer |
| Sarcoidosis | Multiple solid renal masses, potentially coexisting with medullary $Ca^{2+}$; look for thoracic manifestations |
| Birt-Hogg-Dubé | Multiple solid renal masses, with possible ‘spoke-wheel’ morphology; basilar-predominant pulmonary cysts |
| Tuberous sclerosis | Multiple fat-containing solid renal masses and cysts; look for coexisting cystic lung disease (LAM) |
| Von Hippel Lindau | Multiple solid renal masses and cysts; look for cystic lesions in pancreas, pheochromocytoma in adrenals |
| IgG4 disease | Most commonly multiple solid renal masses; look for pancreatitis, biliary strictures, periaortitis |

**Abbreviations:** ADPKD = autosomal dominant polycystic kidney disease; ARKPD = autosomal recessive polycystic kidney disease; ATN = acute tubular necrosis; $Ca^{2+}$ = calcification; ESRD = end-stage renal disease; GPA = granulomatosis with polyangiitis; LAD = lymphadenopathy; LAM = lymphangioleiomyomatosis; MEN = multiple endocrine neoplasia; SLE = systemic lupus erythematosis